Università degli Studi di Siena

Facoltà di Scienze Matematiche Fisiche e Naturali

Tesi di Dottorato in Fisica Sperimentale

PhD Thesis in Experimental Physics

XXIII Ciclo

First Observation of Charmed Resonances in the $\Lambda_b^0 \rightarrow \Lambda_c^+\pi^-\pi^+\pi^-$ Inclusive Decays and Measurement of their Relative Branching Ratios at CDF

Candidate

Patrizia Barria

Advisor

Dott. Maria Agnese Ciocci

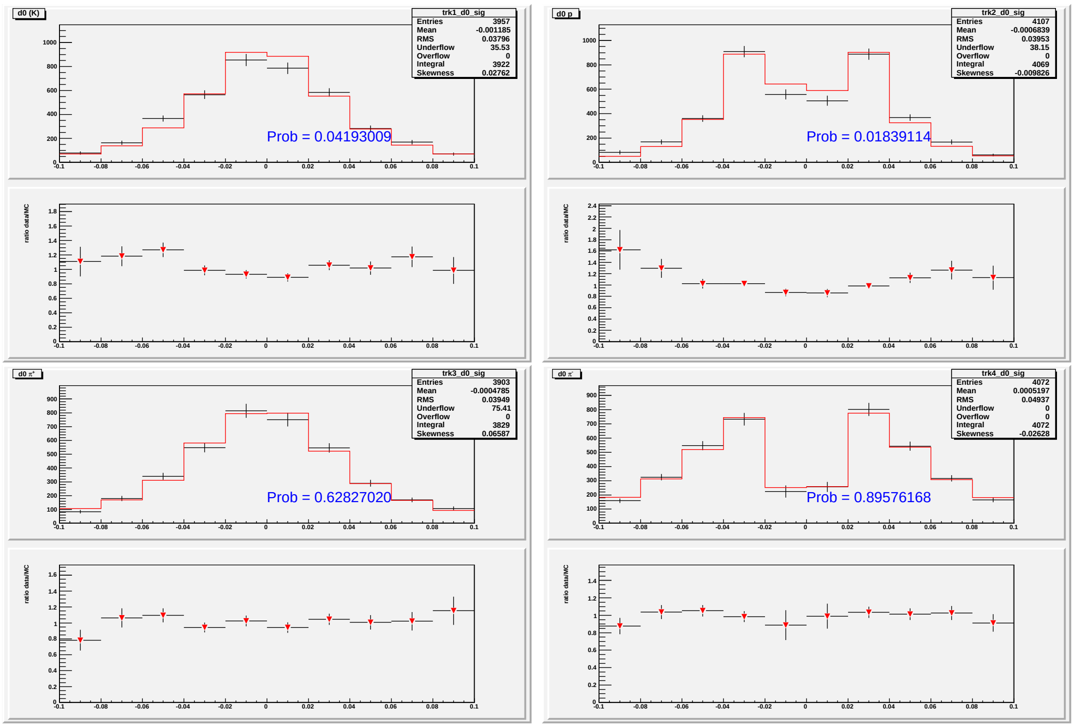

Figure A.8: *d_0 distributions of the four tracks produced in the $\Lambda_b^0 \to \Lambda_c^+\pi^-$ decay for data (black) and MC (red).*

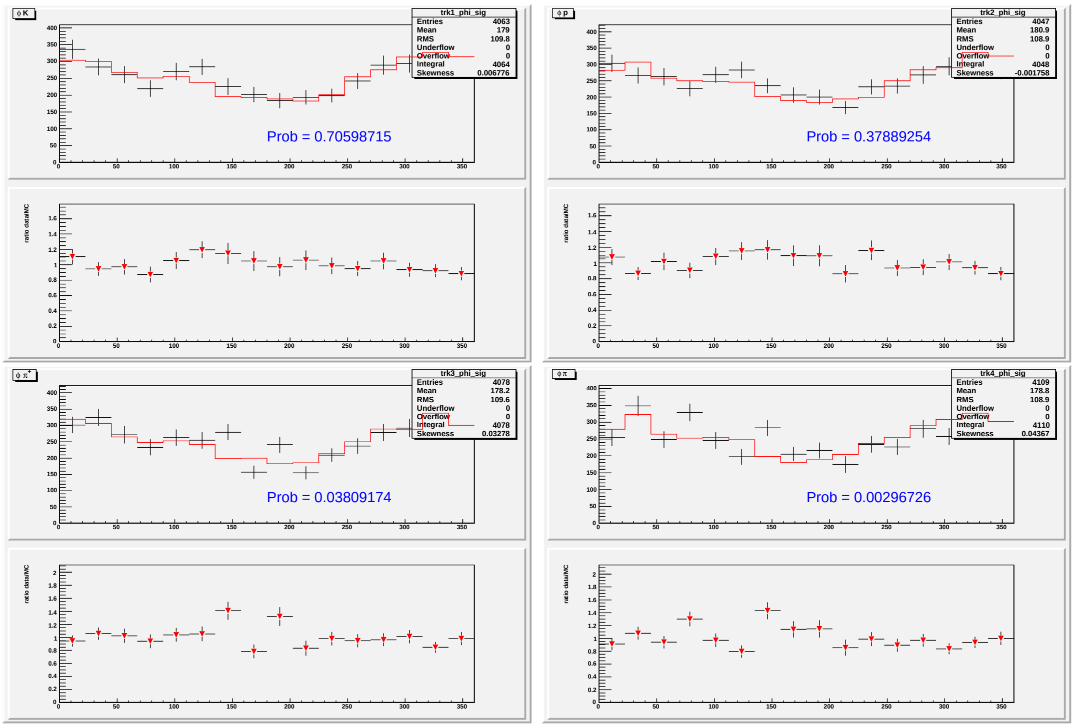

Figure A.9: *φ_0 distributions of the four tracks produced in the $\Lambda_b^0 \to \Lambda_c^+ \pi^-$ decay for data (black) and MC (red).*

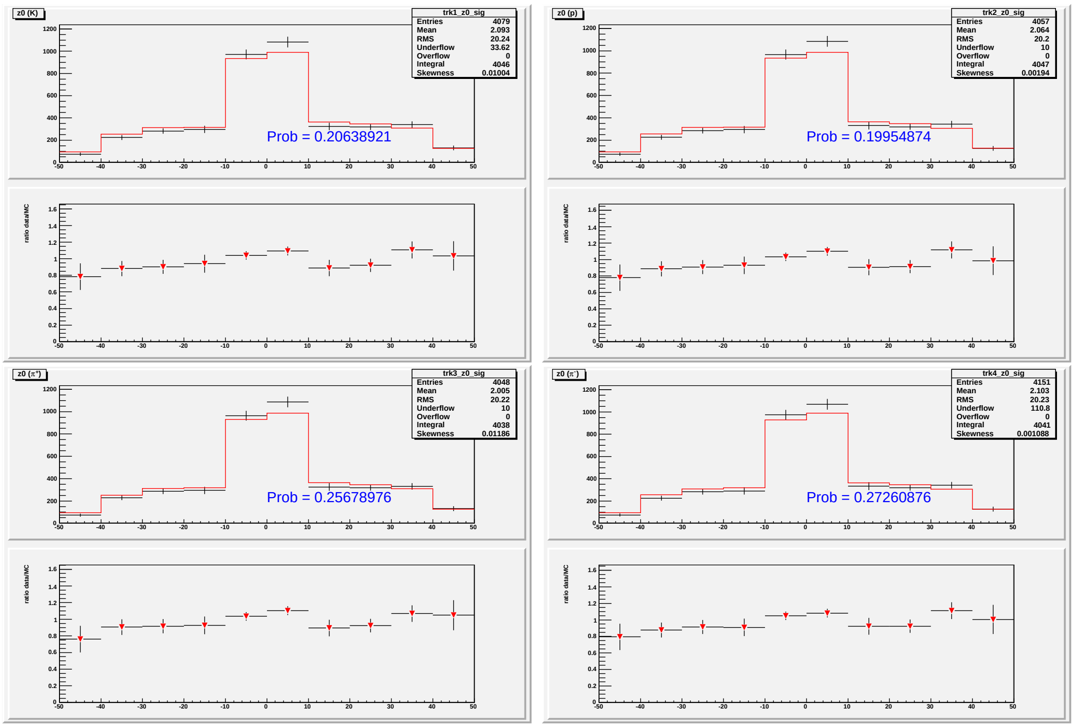

Figure A.10: *z_0 distributions of the four tracks produced in the $\Lambda_b^0 \to \Lambda_c^+\pi^-$ decay for data (black) and MC (red).*

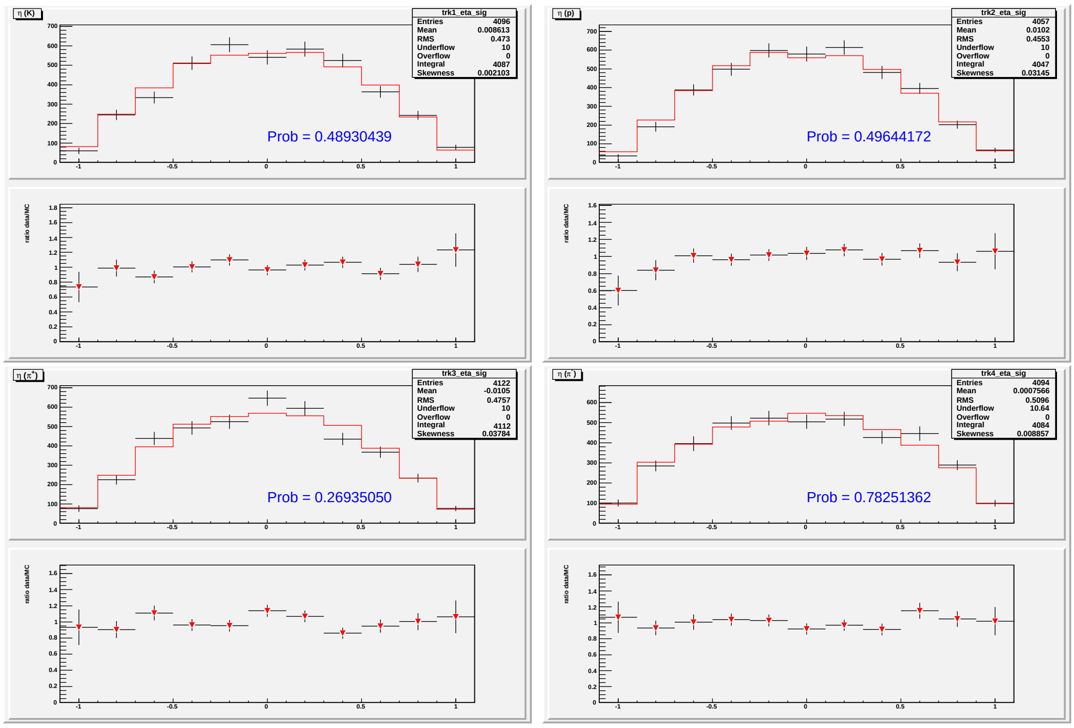

Figure A.11: *η distributions of the four tracks produced in the $\Lambda_b^0 \rightarrow \Lambda_c^+ \pi^-$ decay for data (black) and MC (red).*

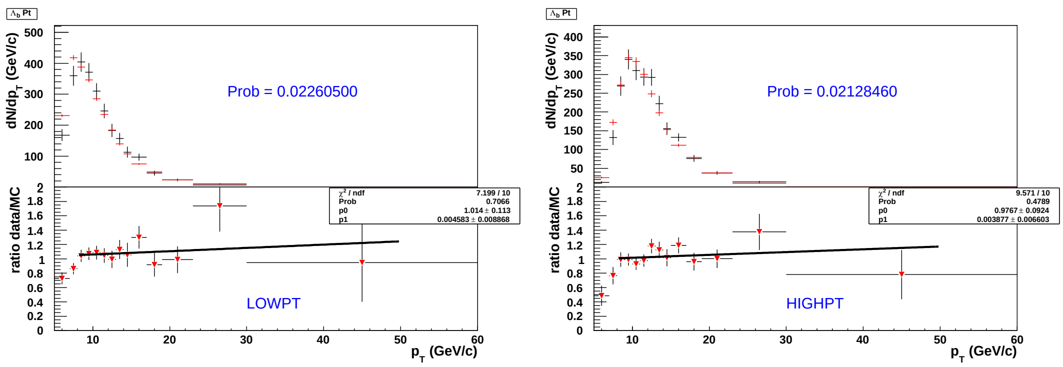

(a)

(b)

Figure A.12: *$p_T(\Lambda_b^0)$ comparison between data and MC for events collected by the B_CHARM_LOWPT trigger* **A.12(a)** *and B_CHARM_HIGHPT trigger* **A.12(b)**.

Appendix **B**

Physics Background Study

In Chap. 5 we extracted the signal yields of the $\Lambda_b^0 \rightarrow \Lambda_c^+\pi^-\pi^+\pi^-$ after the veto on the charmed resonant Λ_b^0 decay modes, with Λ_c^+ into a $pK^-\pi^+$ final state. A not biased extraction of these yields required an accurate modeling of the background shape and in particular of the physical background contributing into the Λ_b^0 mass window.

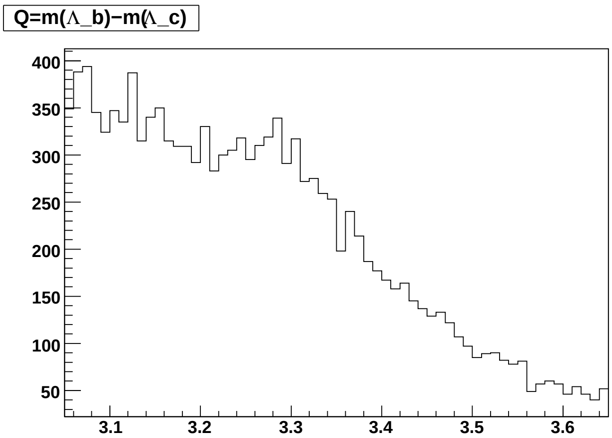

Figure B.1: *ΔM^{--+} MC distribution of $\overline{B}^0_{(s)} \rightarrow D^{(*)+}_{(s)}\pi^-\pi^+\pi^-$ (with inclusive $D^{(*)+}_{(s)}$ decay modes).*

Considering the inclusive $\Lambda_b^0 \rightarrow \Lambda_c^+\pi^-\pi^+\pi^-$ candidates (see Fig. 5.2(a) and Fig. 5.2(b)) and also when the distribution is done for the $\Lambda_b^0 \rightarrow \Lambda_c^+\pi^-\pi^+\pi^-$, by vetoing the $\Lambda_c(2595)^+$, $\Lambda_c(2625)^+$, $\Sigma_c(2455)^{++}$ and $\Sigma_c(2455)^0$ resonances (see Fig. 5.10(a) and

Fig. 5.10(b)), the $\overline{B}^0_{(s)} \rightarrow D^{(*)+}_{(s)}\pi^-\pi^+\pi^-$[1], with inclusive $D^{(*)+}_{(s)}$ decays modes, can be assumed as the main sources of the physical background to the $\Lambda^0_b \rightarrow \Lambda^+_c\pi^-\pi^+\pi^-$ signal. This kind of background occurs, for example, in the $D^+ \rightarrow K^-\pi^+\pi^+$ decay mode when one of the two π^+ produced in the D^+ decay is assigned the proton mass, and the combination of the three particles form an invariant mass compatible with the Λ^+_c so that the combination of the six tracks falls in the Λ^0_b mass region as well for a generic decay with an efficiency dependent on the $D^{(*)+}$ decay mode.

Just as an example, we present here the study done to determine the modeling of the background for the $\Lambda^0_b \rightarrow \Lambda^+_c\pi^-\pi^+\pi^-$ without charmed resonant decay modes (after applying the veto on the charmed resonances). MC distribution are obtained applying the same requirements as for data. Fig. B.1 shows the ΔM^{--+} mass distribution (template) of a MC sample of $\overline{B}^0 \rightarrow D^{(*)+}\pi^-\pi^+\pi^-$ and $\overline{B}^0_s \rightarrow D^{(*)+}_s\pi^-\pi^+\pi^-$ mixed in the proportions expected from the measured f_s/f_d ratio [1] (see Sec. 1.2) and the measured branching fractions [1], when reconstructed as a $\Lambda^0_b \rightarrow \Lambda^+_c\pi^-\pi^+\pi^-$ without charmed resonances candidate.

The distribution peaks in the region around 3.3 GeV/c^2 and this is due to the subsample where the D^+ or D^+_s decay exactly into three charged tracks, as shown repectively in Fig. B.2(a) and Fig. B.2(b) where their ΔM^{--+} distribution is reported.

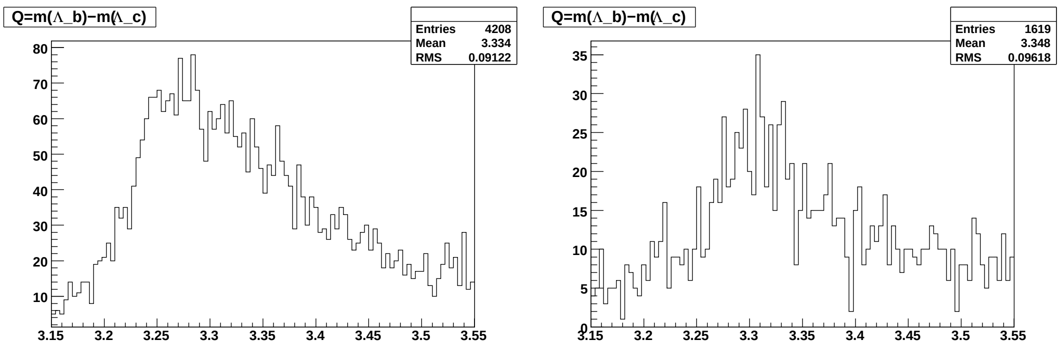

(a) (b)

Figure B.2: *ΔM^{--+} MC distribution of $\overline{B}^0 \rightarrow D^+\pi^-\pi^+\pi^-$* **B.2(a)** *and $\overline{B}^0_s \rightarrow D^+_s\pi^-\pi^+\pi^-$* **B.2(b)** *with D^+ and the D^+_s decays in three charged tracks.*

Fig. B.3(a) shows the ΔM^{--+} distribution for these candidates when the mode-

[1] In the following we indicate with $\overline{B}^0_{(s)} \rightarrow D^{(*)+}_{(s)}\pi^-\pi^+\pi^-$ the four decay modes $\overline{B}^0 \rightarrow D^+\pi^-\pi^+\pi^-$, $\overline{B}^0 \rightarrow D^{*+}\pi^-\pi^+\pi^-$, $\overline{B}^0_s \rightarrow D^+_s\pi^-\pi^+\pi^-$ and $\overline{B}^0_s \rightarrow D^{*+}_s\pi^-\pi^+\pi^-$.

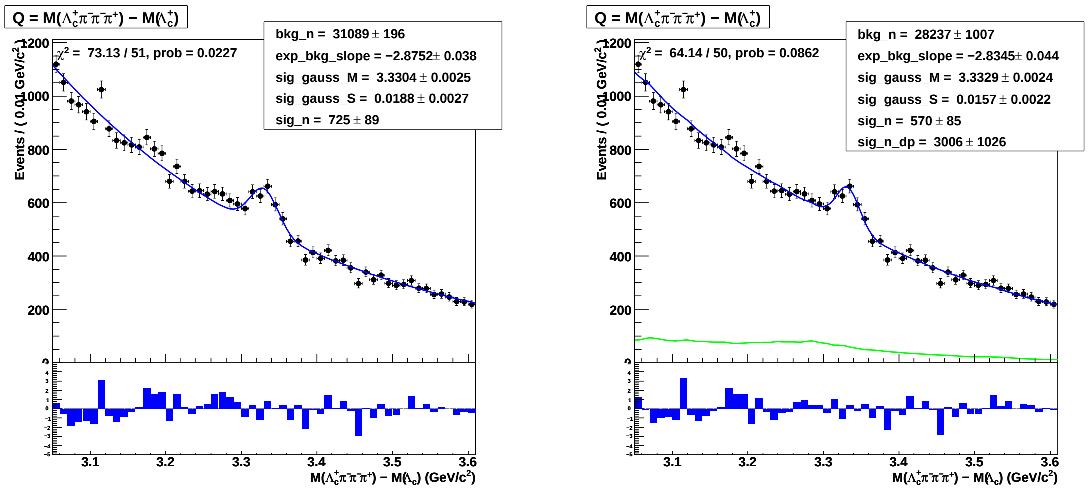

(a) (b)

Figure B.3: **B.3(a):** *Fit of all the* Λ_b^0 *candidates when the resonant decay modes have been removed with the cuts* $\Delta M^{+-} > 0.380$ *GeV/c*^{2}, $\Delta M^{+} > 0.190$ *GeV/c*^{2} *and* $\Delta M^{-} > 0.190$ *GeV/c*^{2}*, the background is modeled using an exponential shape with slope and normalization free to float in the fit.* **B.3(b):** *Unlike the previous plots here have been also included the floating contribution due to* $\overline{B}^0 \rightarrow D^{(*)+}\pi^-\pi^+\pi^-$ *and* $\overline{B}_s^0 \rightarrow D_s^{(*)+}\pi^-\pi^+\pi^-$ *(with inclusive* $D^{(*)+}$ *and* $D_s^{(*)+}$ *decays) with a fixed shape (MC template).*

ling assumes an exponential to model the background and a gaussian to model the signal. In the fit, slope and contribution of the exponential, as well gaussian mean and sigma, are free to float. Fig. B.3(b) shows the distribution of ΔM^{--+} for the Λ_b^0 reconstructed candidates, with overlaid the best fit curve, when we add the modeling of a physical background, described by the templates made for the $\overline{B}_{(s)}^0 \rightarrow D_{(s)}^{(*)+}\pi^-\pi^+\pi^-$, to the exponential, to model the combinatorial background; the slope of the exponential and the normalization of the two background distributions are floating and determined by the fit: the green curve represents the contribution due to the physical background. By comparison of these two figures, the modeling including this physical backround is better (compare the χ^2) and the misreconstructed $\overline{B}_{(s)}^0 \rightarrow D_{(s)}^{(*)+}\pi^-\pi^+\pi^-$ decays contribute significantly to the Λ_b^0 mass window. A similar result is obtained when in the modeling we fix the slope of the exponential, using the high mass region (see Sec. 3.4), and we add, in the modeling of the physical background, also a contribute due to the B^0 inclusive decay modes.

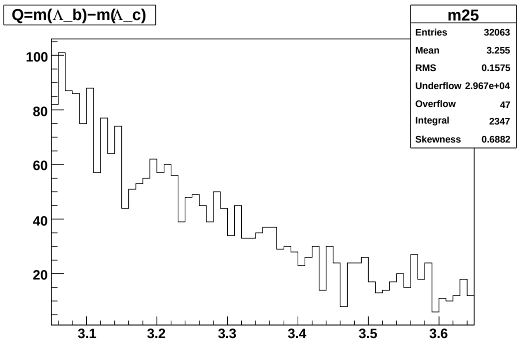

(a)

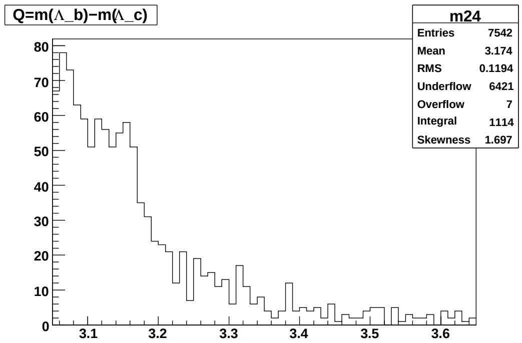

(b)

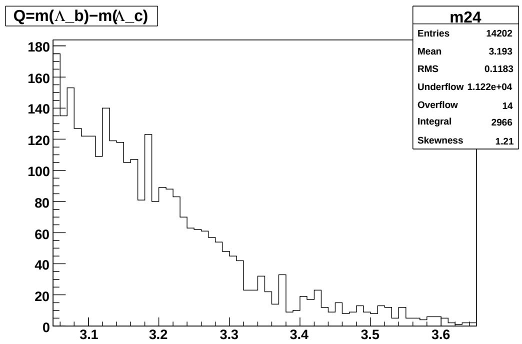

(c)

Figure B.4: *ΔM^{--+} MC distributions of $B^0 \to$ Inclusive* **B.4(a)**, *$\Lambda_b^0 \to \Lambda_c^+\pi^-\pi^+\pi^-\pi^0$* **B.4(b)** *and $\Lambda_b^0 \to \pi^-\pi^+\ell\overline{\nu}_\ell$* **B.4(c)**.

In order to do that, we used a MC sample of $B^0 \to$ Inclusive decays to obtain the corresponding ΔM^{--+} template (see Fig. B.4(a)) when these decays are recontructed as a $\Lambda_b^0 \to \Lambda_c^+\pi^-\pi^+\pi^-$ candidate without charmed resonances. Adding this physical background contribution (fixed shape, as determined by the template and normalization free to float in the fit), the change in the signal yields is negligible. This can be inferred comparing the yield determined by the best fit of ΔM^{--+} data (value of the variable `sig_n` in the fit result legenda) of Fig. B.3(b) with the one of Fig. 5.10(a) for the $\Lambda_b^0 \to \Lambda_c^+\pi^-\pi^+\pi^-$ without charmed resonances with $\Lambda_c^+ \to pK^-\pi^+$. Added this background in the modeling, we verified that futher contribution to the physical background modeling are not significant in the Λ_b^0 mass window. ΔM^{--+} distributions for the MC samples of $\Lambda_b^0 \to \pi^-\pi^+\pi^-\pi^0$

and $\Lambda_b^0 \rightarrow \pi^-\pi^+\ell\overline{\nu}_\ell$, the templates, are shown respectively in Fig. B.4(b) and Fig. B.4(c) and show that these contributions are not significant in the Λ_b^0 mass window.

Cross Check of the Physical Background Modeling using real data

We performed further useful cross-check of the background directly on the data using the Λ_b^0 reconstructed candidates, after the veto on the charmed resonances. Fig. B.3(b) shows the ΔM^{--+} distribution for this sample. Fig. B.5(a) shows the invariant mass spectrum of the $D^+ \rightarrow K^-\pi^+\pi^+$ candidates reconstructed in these data by assigning the kaon and pion masses to the Λ_c^+ candidate decay products $K^-p\pi^+$. The fit estimates a D^+ mass of 1.868 GeV/c^2 and a signal width of 7.5 MeV/c^2. Fig. B.5(b) shows the reconstructed $\overline{B}^0 \rightarrow D^+\pi^-\pi^+\pi^-$ candidates, when we applied the same exact cuts used to reconstruct the Λ_b^0 candidates without charmed resonances.
We estimate a yield of 360±40 B^0 events ($N(B^0)$) in the ΔM^{--+} window $[3.15-3.55]$ GeV/c^2 used for the Λ_b^0 fit. The estimated B^0 mass is (5278 ± 1) MeV/c^2 and the width is (17.5 ± 1.6) MeV/c^2. Since the reconstruction in our data has not been a success for both the D_s^+ and $\overline{B}_s^0 \rightarrow D_s^+\pi^-\pi^+\pi^-$ signals, we decided to estimate the total contribution expected from this source relative to the estimated yield of 360±40 $\overline{B}^0 \rightarrow D^+\pi^-\pi^+\pi^-$ events. Since the MC estimates a relative efficiency $\varepsilon(B_s^0)/\varepsilon(B^0) = 1.35$, we can give a raw estimate of the expected B_s^0 yield ($N(B_s^0)$) using the following formula where for the BR of each decay we used the corresponding PDG value:

$$N(B_s^0) = N(B^0) \times \frac{f_s}{f_d} \times \frac{\mathcal{B}(\overline{B}_s^0 \rightarrow D_s^+\pi^-\pi^+\pi^-)}{\mathcal{B}(\overline{B}^0 \rightarrow D^+\pi^-\pi^+\pi^-)} \times \frac{\mathcal{B}(D_s^+ \rightarrow K^+K^-\pi^+ \ or\ \pi^-\pi^+\pi^-)}{\mathcal{B}(D^+ \rightarrow K^-\pi^+\pi^+)} \times \frac{\varepsilon(B_s^0)}{\varepsilon(B^0)} \tag{B.1}$$

$$N(B_s^0) = 360 \times \frac{0.118}{0.323} \times 1.05 \times \frac{0.066}{0.092} \times 1.35 = 133 \tag{B.2}$$

The reconstructed ΔM^{--+} distribution of the MC sample of $\overline{B}^0 \rightarrow D^+\pi^-\pi^+\pi^-$and $\overline{B}_s^0 \rightarrow D_s^+\pi^-\pi^+\pi^-$ signals, in the expected proportions, is reported in Fig. B.6(a): this background covers the entire $[3.15-3.55]$ GeV/c^2 window.
In the fit, this distribution is then used as template to model the physical background while an exponential is used to model the combinatorial background. The physical background normalization is given by the sum of the 360 $\overline{B}^0 \rightarrow D^+\pi^-\pi^+\pi^-$ and of the 133 $\overline{B}_s^0 \rightarrow D_s^+\pi^-\pi^+\pi^-$ which gives a total of 493 events, while the slope and the normalization of the exponential are free to float in the fit.

The best fit returns a Λ_b^0 yield of 596±78 signal events (value of `sig_n` in the fit results legenda of Fig. B.6(b)), which is consistent with the yield of $\Lambda_b^0 \to \Lambda_c^+\pi^-\pi^+\pi^-$ without charmed resonances signal events, when the modeling is done using the procedure described in Sec. 5.3 but in the enlarged range of mass, $[3.15 - 3.55]$ GeV/c^2 (see Fig. 5.10(a), `sig_n` value in the fit results legenda). We have also performed the same fit with floating $\overline{B}^0 \to D^+\pi^-\pi^+\pi^-$ and $\overline{B}_s^0 \to D_s^+\pi^-\pi^+\pi^-$ backgrounds (Fig. B.6(c)) and the estimate of the signal and background yields are consistent with the central result.

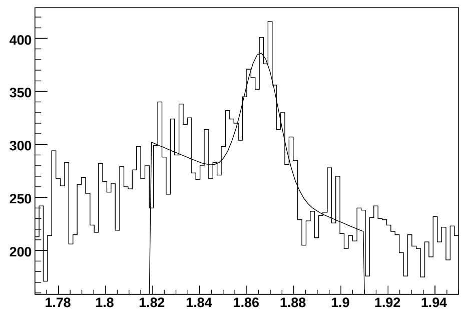

(a)

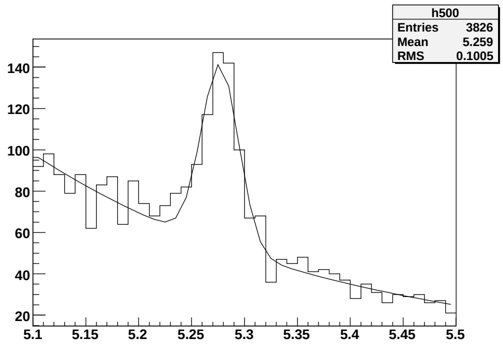

(b)

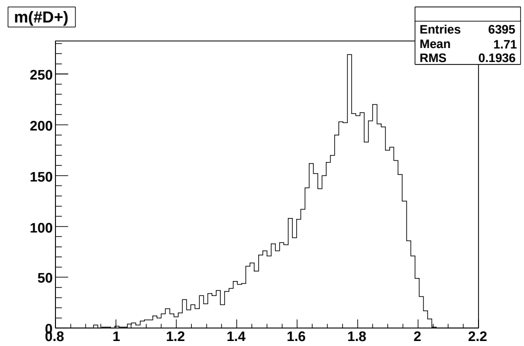

(c)

Figure B.5: **B.5(a):** *D^+ signal reconstructed in data by assigning the kaon and pion masses to the Λ_c^+ decay products.* **B.5(b):** *$\overline{B}^0 \to D^+\pi^-\pi^+\pi^-$ signal reconstructed in data by using the D^+ signal (to reconstruct this signal we applied the cut $|\, m(D^+) - 1.868\, | < 0.022\,\mathrm{GeV/c^2}$).* **B.5(c):** *MC mass distribution of the Λ_c^+ (from Λ_b^0) reconstructed as D^+.*

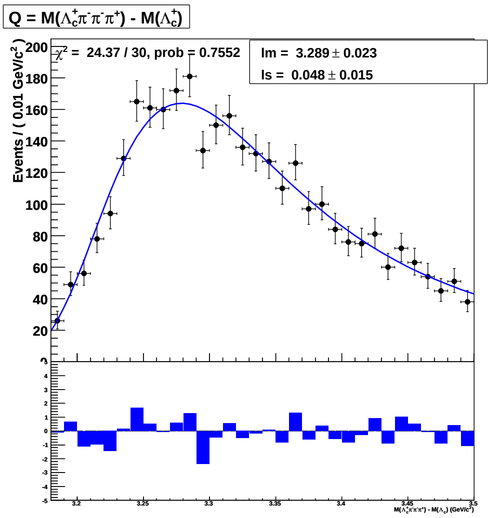

(a)

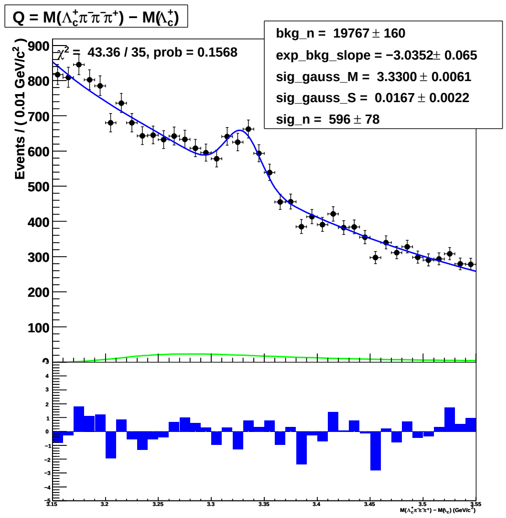

(b)

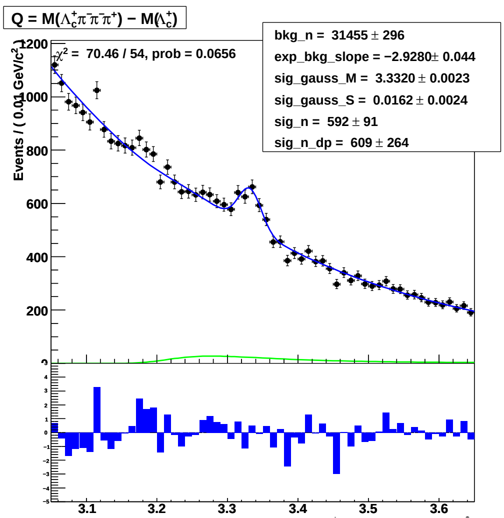

(c)

Figure B.6: **B.6(a)**: *Reconstructed ΔM^{--+} distribution of the MC sample of $\overline{B}^0_{(s)} \to D^+_{(s)}\pi^-\pi^+\pi^-$ signals in the expected proportions.* **B.6(b)**: *Fit of all the Λ^0_b candidates: resonant decay modes removed with the cuts $\Delta M^{+-} > 0.380\,\mathrm{GeV/c^2}$, $\Delta M^{+} > 0.190\,\mathrm{GeV/c^2}$ and $\Delta M^{-} > 0.190\ GeV/c^2$ and the B^0 and B^0_s contribution fixed to 493 events.* **B.6(c)**: *Fit of all the Λ^0_b candidates, including the the B^0 and B^0_s background left floating and determined by the fit.*

Appendix C

MC Estimate of the Cabibbo Suppressed decay modes contributions

In order to determine the yields of the Λ_b^0 in the $\Lambda_b^0 \to \Lambda_c^+\pi^-\pi^+\pi^-$ mass spectra, we need a good assessment of the backgrounds which reside under the Λ_b^0 signal peak. One such class of backgrounds are the CS decay modes, where one of the π^- is replaced by a K^-. In the following we estimate the ratios of the BRs of the CS to the CF decay modes, and estimate the fraction of CS background to the CF in all decay modes reported in Tab. C.1. We provide similar estimates for the CS background relatively to the decay $\Lambda_b^0 \to \Lambda_c^+\pi^-$. These ratios of BRs are used in Chap. 5 to estimate the expected yield of the CS background corresponding to a given yield of the CF decay mode, once the respective efficiencies are known from simulated samples. Here we give an example of how the expected contamination of a CS decay mode can be evaluated when the signal is reconstructed as the corresponding CF decay mode. We remember that the CS decay modes are not modeled in the physical background (see section Sec. 5.1), since we expect very few events, but are assumed as a systematic affecting the corresponding CF yields (see Sec. 7.1.1).

Outline

The yields of the Λ_b^0 decay modes, extracted by the fit procedure described in Chap. 5 applied to the ΔM^{--+} mass distribution, are determined assuming no contribution from the CS decay modes. The observed signals in the ΔM^{--+} mass distribution, for each decay mode, have two contributions: the CF and the CS. Denoting with N^i_{obs} the yield of the i^{th} decay mode extracted, and with N^i_{CS} and

N^i_{CF} the corresponding contributions of the CS and of the CF we can write:

$$N^i_{obs} = N^i_{CF}(1 + N^i_{CS}/N^i_{CF}) \tag{C.1}$$

Λ_b^0 Cabibbo favored decay modes	Λ_b^0 Cabibbo suppressed decay modes
$\Lambda_b^0 \to \Lambda_c^+\pi^-$	$\Lambda_b^0 \to \Lambda_c^+K^-$
$\Lambda_b^0 \to \Lambda_c^+\pi^-\pi^-\pi^+$	$\Lambda_b^0 \to \Lambda_c^+\pi^+\pi^-K^-$
$\Lambda_b^0 \to \Lambda_c^*(2595)^+\pi^-$	$\Lambda_b^0 \to \Lambda_c^*(2595)^+K^-$
$\Lambda_b^0 \to \Lambda_c^*(2625)^+\pi^-$	$\Lambda_b^0 \to \Lambda_c^*(2625)^+K^-$
$\Lambda_b^0 \to \Sigma_c(2455)^{++}\pi^-\pi^-$	$\Lambda_b^0 \to \Sigma_c(2455)^{++}\pi^-K^-$
$\Lambda_b^0 \to \Sigma_c(2455)^0\pi^-\pi^+$	$\Lambda_b^0 \to \Sigma_c(2455)^0\pi^+K^-$
$\Lambda_b^0 \to \Lambda_c^+\rho^0\pi^-$	$\Lambda_b^0 \to \Lambda_c^+\rho^0K^-$

Table C.1: *CF and CS decay modes.*

The amount of CS background we expect, relative to the CF signals, for each decay mode i in Tab. C.1, is given by the expression:

$$\frac{N^i_{CS}}{N^i_{CF}} = \frac{\mathcal{B}(\Lambda_b^0 \to CS^i) \times \varepsilon^i_{CS}}{\mathcal{B}(\Lambda_b^0 \to CF^i) \times \varepsilon^i_{CF}} \tag{C.2}$$

where ε^i is the efficiency of reconstructed signal in mode i and $\mathcal{B}(\Lambda_b^0 \to CS^i)$ and $\mathcal{B}(\Lambda_b^0 \to CF^i)$ is the BR of the Λ_b^0 in the CS and in the corresponding CF decay modes. From Eq. C.2, in order to estimate N^i_{CS}/N^i_{CF}, we need to know the relative efficiency estimates and the relative BRs ($\mathcal{B}$) of each decay mode. In the following we describe the studies done for these estimates.

Evaluation of $\mathcal{B}(\Lambda_b^0 \to CS^i)$

The CS decay modes for which we need BR have not been observed, let alone measured. The decay amplitude, for the baryonic CF decay mode, is $\propto |V_{ud}|^2$ while is $\propto |V_{us}|^2$ for the CS one. If we consider the decay amplitude for the related mesonic decay mode, we find the same number in both cases, CF and CS decay modes. We estimate the ratio $\mathcal{B}(\Lambda_b^0 \to CS^i)/\mathcal{B}(\Lambda_b^0 \to CF^i)$ either using similar decay modes observed in B-mesons, where the measurements already exist (from the B-Factories or CDF itself), or, when these measurements are not available, simply using the ratio $|V_{ud}|^2/|V_{us}|^2$.

Just as an example, to illustrate the concepts described above, we estimate the CS $\mathcal{B}(\Lambda_b^0 \to \Sigma_c(2455)^0\pi^+K^-)$ relative to the CF decay $\Lambda_b^0 \to \Sigma_c(2455)^0\pi^+\pi^-$. The first order Feynman diagram of this decay, for the CF and for the corresponding CS, is reported in Fig. C.1.

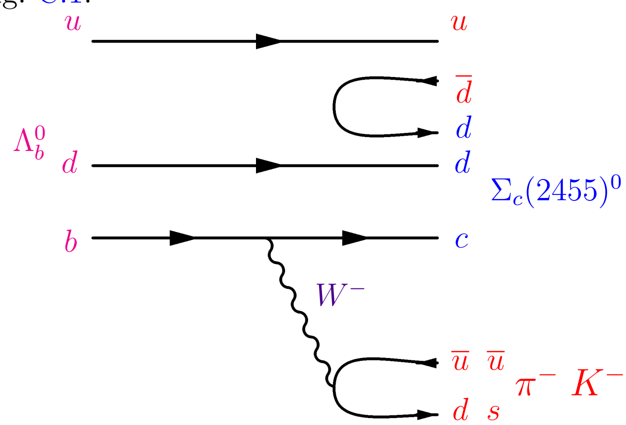

Figure C.1: *Feynman diagram illustrating the decays $\Lambda_b^0 \to \Sigma_c(2455)^0\pi^+\pi^-$ and $\Lambda_b^0 \to \Sigma_c(2455)^0\pi^+K^-$.*

The neutral B-meson decay modes, corresponding to the baryonic one of Fig. C.1, are reported in Fig. C.2 and Fig. C.3. The diagrams of Fig. C.2 are obtained removing the line of the Λ_b^0 u quark (one of the spectator quark) in Fig. C.1 and changing, in the same figure, the Λ_b^0 d quark in a $\overline{d}$ quark. The only difference in these two diagrams is that in one case (see Fig. C.2**(b)**) the gluon splits in a $u\overline{u}$ pair, while in the other (see Fig. C.2**(a)**) in a $d\overline{d}$ pair.

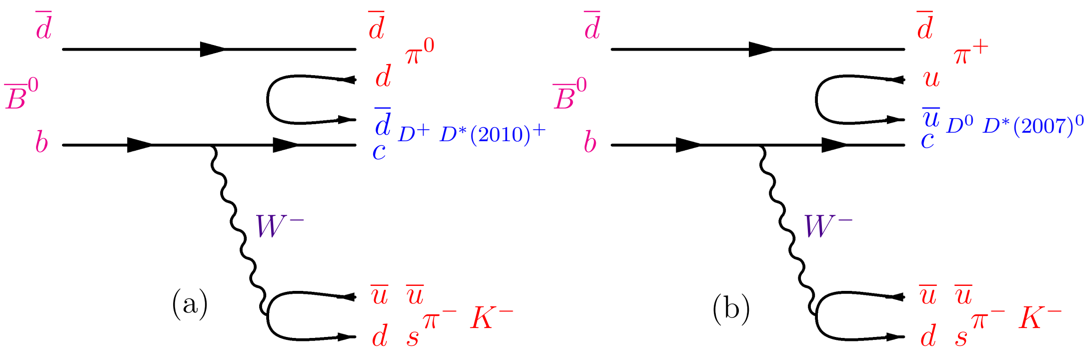

Figure C.2: *Feynman diagrams illustrating the neutral B-meson decay modes corresponding to the baryonic decay mode on Fig. C.1.*

Using the same method, the two lower order Feynman diagrams for charged B-meson decay modes are obtained removing the line of the Λ_b^0 d quark (one of the spectator quark) in Fig. C.1 and changing in the same figure the Λ_b^0 u quark in a $\overline{u}$ quark. As before, the only difference in these two diagrams is that in one case (see Fig. C.3(b)) the the gluon splits in a $u\overline{u}$ pair and in the other (see Fig. C.3(a)) in a $d\overline{d}$ pair. So, in principle the Feynman diagrams in Fig. C.2(a), Fig. C.2(b), Fig. C.3(a) and Fig. C.3(b) are equivalent and we can choose anyone of them to made our estimate.

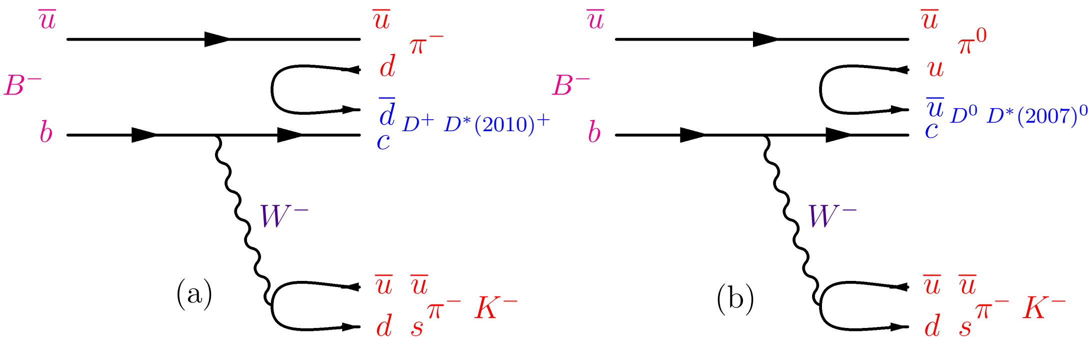

Figure C.3: *Feynman diagrams illustrating the charged B-meson decay modes corresponding to the baryonic decay mode on Fig. C.1.*

In this specific case in our calculation we used, to estimate $\mathcal{B}(\Lambda_b^0 \to \Sigma_c(2455)^0\pi^+K^-)/\mathcal{B}(\Lambda_b^0 \to \Sigma_c(2455)^0\pi^+\pi^-)$, the branching fractions of the decays $B^- \to D^+\pi^-\pi^-$ (S-wave) , $B^- \to D^*(2010)^+\pi^-\pi^-$ (P-wave) and of the corresponding CS decays, which are all measured [1]. The Feynman diagram associated to these decays is the one of Fig. C.3(a). This is due to the fact that the spin 1/2 Λ_b^0 decays into a spin 1/2 Λ_c^+ and, from angular momentum conservation, we expect contributions from both S and P wave amplitudes.
The correspondence between the baryonic and mesonic decay modes here considered, is unfolded as follows:

gluon splits to a $d\overline{d}$ pair;

the decay rate for the baryonic CF decay mode is $\propto |V_{ud}|^2\, |V_{bc}|^2\, |f_1^2|$;

the decay rate for the baryonic CS decay mode is $\propto |V_{us}|^2\, |V_{bc}|^2\, |f_2^2|$;

the decay rate for the mesonic CF decay modes is $\propto |V_{ud}|^2\, |V_{bc}|^2\, |f_3^2|$;

the decay rate for the mesonic CS decay modes is $\propto |V_{us}|^2\, |V_{bc}|^2\, |f_4^2|$.

Therefore, it's easy to understand that each relative branching ratio $\mathcal{B}$ is given by:

$$\underbrace{\frac{|V_{us}|^2\, |V_{bc}|^2\, |f_2^2|}{|V_{ud}|^2\, |V_{bc}|^2\, |f_1^2|}}_{\text{baryonic decay mode}} = \underbrace{\frac{|V_{us}|^2\, |V_{bc}|^2\, |f_4^2|}{|V_{ud}|^2\, |V_{bc}|^2\, |f_3^2|}}_{\text{mesonic decay mode}} \tag{C.3}$$

where $f_3 = f_1$ and $f_4 = f_2$. Since the amplitude for the baryonic decay considered in this example includes contributions from both S-wave ($J = 0$) and P-wave ($J = 1$) transitions then, in the case of mesons, f_3 and f_4 actually have two components :

$$\begin{aligned} f_3 &= f_3(S) + f_3(P) \\ f_4 &= f_4(S) + f_4(P) \end{aligned} \tag{C.4}$$

Looking at the Eq. C.3 we have to add the two terms and then square them to get the cross terms:

$$\begin{aligned} |f_3|^2 &= |f_3(S)|^2 + |f_3(P)|^2 + \underbrace{(f_3^*(S))(f_3(P)) + (f_3(S))(f_3^*(P))}_{\text{negligible}} \\ |f_4|^2 &= |f_4(S)|^2 + |f_4(P)|^2 + \underbrace{(f_4^*(S))(f_4(P)) + (f_4(S))(f_4^*(P))}_{\text{negligible}} \end{aligned} \tag{C.5}$$

Combining Eq. C.3 and Eq. C.5 and assuming negligible the cross terms, we get:

$$\frac{\mathcal{B}^{(CS)}_{baryon}}{\mathcal{B}^{(CF)}_{baryon}} = \frac{|V_{us}|^2\ (|f_4(S)|^2 + |f_4(P)|^2)}{|V_{ud}|^2\ (|f_3(S)|^2 + |f_3(P)|^2)} = \frac{\mathcal{B}^{(CS)}_{meson\ (S)} + \mathcal{B}^{(CS)}_{meson\ (P)}}{\mathcal{B}^{(CF)}_{meson\ (S)} + \mathcal{B}^{(CF)}_{meson\ (P)}} \tag{C.6}$$

We applied this method to all studied decay modes once known the corresponding B-meson decays modes contributing.

Therefore, in the example of the $\Lambda_b^0 \to \Sigma_c(2455)^0\pi^+K^-$ and $\Lambda_b^0 \to \Sigma_c(2455)^0\pi^+\pi^-$, considering the contributions of all the corresponding B-meson decays modes Feynman diagrams we have:

$$\begin{aligned} &\frac{\mathcal{B}(\Lambda_b^0 \to \Sigma_c(2455)^0\pi^+K^-)}{\mathcal{B}(\Lambda_b^0 \to \Sigma_c(2455)^0\pi^+\pi^-)} = \frac{\mathcal{B}(B^- \to D^+\pi^-K^-) + \mathcal{B}(B^- \to D(2010)^{*+}\pi^-K^-)}{\mathcal{B}(B^- \to D^+\pi^-\pi^-) + \mathcal{B}(B^- \to D(2010)^{*+}\pi^-\pi^-)} \\ &= \frac{(0.55 \pm 0.54) \times 10^{-4} + (0.73 \pm 0.54) \times 10^{-4}}{(1.02 \pm 0.16) \times 10^{-3} + (1.35 \pm 0.22) \times 10^{-3}} \\ &= \frac{(1.28 \pm 0.76) \times 10^{-4}}{(2.37 \pm 0.27) \times 10^{-3}} \\ &= (5.40 \pm 3.26) \times 10^{-2} \end{aligned} \tag{C.7}$$

where all the used $\mathcal{B}$ are from PDG [1].
Tab. C.2 summarizes as input the B-meson decay modes contributing to the CF

Meson Decay	$\mathcal{B}$ (PDG)	Λ_b^0 decay mode	Sum of CF/CS $\mathcal{B}$
$\overline{B}^0 \to D^*(2010)^+\pi^-$	$(2.76 \pm 0.13) \times 10^{-3}$	$\Lambda_b^0 \to \Lambda_c^*(2595)^+\pi^-$	$(2.76 \pm 0.13) \times 10^{-3}$
$\overline{B}^0 \to D^*(2010)^+K^-$	$(2.14 \pm 0.16) \times 10^{-4}$	$\Lambda_b^0 \to \Lambda_c^*(2595)^+K^-$	$(2.14 \pm 0.16) \times 10^{-4}$
$\overline{B}^0 \to D^*(2010)^+\pi^-$	$(2.76 \pm 0.16) \times 10^{-3}$	$\Lambda_b^0 \to \Lambda_c^*(2625)^+\pi^-$	—
$\overline{B}^0 \to D_2^*(2460)^+\pi^-$	*not in PDG 2008*		
$\overline{B}^0 \to D^*(2010)^+K^-$	$(2.14 \pm 0.16) \times 10^{-4}$	$\Lambda_b^0 \to \Lambda_c^*(2625)^+K^-$	—
$\overline{B}^0 \to D_2^*(2460)^+K^-$	*not in PDG 2008*		
$\overline{B}^0 \to D^0\pi^+\pi^-$	$(8.40 \pm 0.90) \times 10^{-4}$	$\Lambda_b^0 \to \Sigma_c(2455)^{++}\pi^-\pi^-$	$(14.60 \pm 2.40) \times 10^{-4}$
$\overline{B}^0 \to D^*(2007)^0\pi^+\pi^-$	$(6.20 \pm 2.20) \times 10^{-4}$		
$\overline{B}^0 \to D^0\pi^+K^-$	$(8.80 \pm 1.70) \times 10^{-5}$	$\Lambda_b^0 \to \Sigma_c(2455)^{++}\pi^-K^-$	$(12.10 \pm 5.70) \times 10^{-5}$
$\overline{B}^0 \to D^*(2007)^0\pi^+K^-$	$(3.34 \pm 5.40) \times 10^{-5}$ [a]		
$B^- \to D^+\pi^-\pi^-$	$(1.02 \pm 0.16) \times 10^{-3}$	$\Lambda_b^0 \to \Sigma_c(2455)^0\pi^+\pi^-$	$(2.37 \pm 0.27) \times 10^{-3}$
$B^- \to D^*(2010)^+\pi^-\pi^-$	$(1.35 \pm 0.22) \times 10^{-3}$		
$B^- \to D^+\pi^-K^-$	$(0.55 \pm 0.54) \times 10^{-4}$ [a]	$\Lambda_b^0 \to \Sigma_c(2455)^0\pi^+K^-$	$(1.28 \pm 0.76) \times 10^{-4}$
$B^- \to D^*(2010)^+\pi^-K^-$	$(0.73 \pm 0.54) \times 10^{-4}$ [a]		
$\overline{B}^0 \to D^+\rho^0\pi^-$	$(1.10 \pm 1.00) \times 10^{-3}$	$\Lambda_b^0 \to \Lambda_c^+\rho^0\pi^-$	$(1.10 \pm 1.00) \times 10^{-3}$
$\overline{B}^0 \to D^+\rho^0K^-$	$(0.59 \pm 0.55) \times 10^{-4}$ [a]	$\Lambda_b^0 \to \Lambda_c^+\rho^0K^-$	$(0.59 \pm 0.55) \times 10^{-4}$
$B^- \to D^0\pi^-\pi^+\pi^-$	$(5 \pm 4) \times 10^{-3}$	$\Lambda_b^0 \to \Lambda_c^+\pi^-\pi^+\pi^-$	$(15.3 \pm 4.18) \times 10^{-3}$
$B^- \to D^*(2007)^0\pi^-\pi^+\pi^-$	$(1.03 \pm 0.12) \times 10^{-2}$		
$B^- \to D^0\pi^+\pi^-K^-$	$(2.70 \pm 0.74) \times 10^{-4}$ [a]	$\Lambda_b^0 \to \Lambda_c^+\pi^-\pi^+K^-$	$(8.26 \pm 0.69) \times 10^{-4}$
$B^- \to D^*(2007)^+\pi + \pi^-K^-$	$(5.56 \pm 0.66) \times 10^{-4}$ [a]		
$\overline{B}^0 \to D^+\pi^-$	$(2.68 \pm 0.13) \times 10^{-3}$	$\Lambda_b^0 \to \Lambda_c^+\pi^-$	$(5.44 \pm 0.18) \times 10^{-3}$
$\overline{B}^0 \to D^*(2010)^+\pi^-$	$(2.76 \pm 0.13) \times 10^{-3}$		
$\overline{B}^0 \to D^+K^-$	$(2.0 \pm 0.6) \times 10^{-4}$	$\Lambda_b^0 \to \Lambda_c^+K^-$	$(4.14 \pm 0.62) \times 10^{-4}$
$\overline{B}^0 \to D^*(2010)^+K^-$	$(2.14 \pm 0.16) \times 10^{-4}$		

Table C.2: *List of CF and CS B-meson decay modes, the corresponding BR from PDG [1], baryonic Λ_b^0 decay modes and sum of BRs for the CF and CS associated B-meson decay modes.*

[a] These $\mathcal{B}$ are not in PDG [1] so that we evaluated them using Eq. C.8

and to the CS (Meson decay) , the corresponding BR ($\mathcal{B}(PDG)$), the corresponding Λ_b^0 decay mode, in which they are used (Λ_b^0 decay mode) and the sum of the BRs of the B-mesons contributing to the CF and to the CS (Sum of CF/CS $\mathcal{B}$).
The contributing mesonic decay modes were determined for the other Λ_b^0 decay modes using the same method adopted in this example. Some of the $\mathcal{B}$ for B-meson decays have not yet been measured and in this case we use the ratio in Eq. C.8:

$$\frac{\mathcal{B}(CS^i)}{\mathcal{B}(CF^i)} = \frac{|V_{us}|^2}{|V_{ud}|^2} \tag{C.8}$$

MC Evaluated Relative Efficiencies

We used MC samples to evaluate the efficiency for each decay mode of Tab. C.1. There are several components in the MC simulation:

- production and decay of the b-hadrons;

- detector simulation;
- trigger simulation;
- reconstruction.

In this example we give just an early estimate of how the efficiency can be evaluated and we use here a generator-level simulation. We generate 10^6 Λ_b^0 decays in each of the CF and CS modes of Tab. C.1 and we apply similar selections as those described in Chap. 4. Details of the simulation and efficiency calculation for this examle are given in the following sections.

Generating and Decaying b-hadrons with MC

This step is very similar to the one described in Sec. 3.2.1. We estimate the contribution of CS backgrounds to the decays previously listed in Tab. C.1 by generating MC samples containing 10^6 events of single Λ_b^0 hadrons, with a p_T threshold of 5 GeV/c and a pseudo-rapidity range $|\eta| < 1.2$ using the `BGenerator` package [89]. Single Λ_b^0's are generated using a p_T vs rapidity (y) spectrum modified to match the p_T spectrum observed in fully reconstructed $\Lambda_b^0 \to \Lambda_c^+\pi^-$ decays. Because we use a particle spectrum rather than the quark spectrum, as input to `BGenerator`, fragmentation must be explicitly turned off. We force each generated Λ_b^0 to decay through a single and specified decay chain using the `EvtGen` decay package [98] and a user defined decay Table. Also phase space model is used for all baryon decays. In addition, all Λ_c^+ are forced to decay into the $pK^-\pi^+$ final state including the resonance structures as measured by Aitala, et al. [99]. CDF software version 6.1.4mc was used to generate the b-hadrons decays. The information for each event is written in an HEPG Bank, containing full information about them. For each decay mode, a file containing the HEPG Bank is then written and converted to `ROOT` n-tuples for further analysis.

Candidate Requirements

The data used in the analysis subject of this Thesis have been collected by the TTT, specialized to select multibody b-hadronic decay modes. To emulate the trigger, in this study we require that one of the tracks from the Λ_c^+ and one of the Λ_b^0 decay products each pass the requirements for an SVT track with a $p_T > 2$ GeV/c, $0.0120 < |d_0| < 0.1$ cm and a pseudo-rapidity $|\eta| < 1.0$. For the pair of tracks we don't have any requirement on charge combination, $2° < \Delta\varphi_0 < 90°$, $p_{T_1} + p_{T_2} > 5$ GeV/c and $L_{xy} > 0.02$ cm. The common requirements of skimming and analysis are summarized in Tab. C.3 and are the same for $\Lambda_b^0 \to \Lambda_c^+\pi^-$, $\Lambda_b^0 \to \Lambda_c^+\pi^-\pi^+\pi^-$ and their associated CS decay modes. Two further requirements are applied to select $\Lambda_b^0 \to \Lambda_c^+\pi^-\pi^+\pi^-$ and the associated CS decay: the three tracks from the Λ_b^0's decay vertex have to be in a cone fixed by $\Delta R = \sqrt{\Delta\eta^2 + \Delta\varphi^2}$ and the decay length of the Λ_b^0 candidate, projected in the transverse plane, has to be $L_{xy} > 0.02$ cm.

Summary of common requirements	
All tracks η	$\lvert\eta\rvert < 1$
All tracks d_0	$\lvert d_0\rvert < 0.2\ cm$
$p_{T_{\Lambda_b^0\ candidate}}$	$p_{T_{\Lambda_b^0}} > 8$ GeV/c
Λ_b^0 candidate L_{xy}	$L_{xy} > 0.02\ cm$
Triggering tracks	one track from Λ_b^0 and one from Λ_c^+ are SVT trigger tracks

Table C.3: *Common requirements for the selection $\Lambda_b^0 \to \Lambda_c^+\pi^-$, $\Lambda_b^0 \to \Lambda_c^+\pi^-\pi^+\pi^-$ and corresponding CS decay modes.*

With reference to Eq. C.2 the efficiency of each decay mode is calculated as:

$$\varepsilon_i = \frac{N^i_{reco}}{N^i_{gen}} \tag{C.9}$$

where N^i_{reco} is the number of events reconstructed, and N^i_{gen} is the number of events generated in the corresponding decay mode. We evaluated the efficiency after applying the trigger and the analysis requirements for both $\Lambda_c^+\pi^-$ and $\Lambda_c^+\pi^-\pi^+\pi^-$ selections, as reported in Tab. C.4.
To know how many events satisfy the overall selection, we use the information from the generated ntuples and analyze the histograms (see Fig. C.4, Fig. C.5, and Fig. C.6) to determine the number of these events (see Tab. C.5). The total efficiency of each decay mode is achieved by multiplying the efficiency values relative to each kind of selection (trigger and analysis).

Estimated Relative Branching Ratio

Once evaluated $\mathcal{B}(\Lambda_b^0 \to CS^i)/\mathcal{B}(\Lambda_b^0 \to CF^i)$ and $\varepsilon^i_{CS}/\varepsilon^i_{CF}$, after the overall selection (see Tab. C.5), we can estimate the amount of CS background we expect relative to the CF signal using Eq. C.2. The invariant mass spectrum, for each CS and CF decay mode is reported in Fig. C.4, Fig. C.5 and Fig. C.6. In Fig. C.4 and Fig. C.5 are shown the $\Lambda_c^+\pi^-\pi^+\pi^-$ invariant mass spectra for each CF (dashed blue line) and corresponding CS (continuous red line) decay mode after the trigger and the $\Lambda_c^+\pi^-\pi^+\pi^-$ selection. Note well, for the $\Lambda_b^0 \to \Lambda_c^+\pi^-\pi^+\pi^-$ in Fig. C.5(b), the generated CF events are 1/3 of the CS one. In Fig. C.6 is shown, for $\Lambda_c^+\pi^-$

decay mode	TTT effic.($\times 10^{-2}$)	$\Lambda_c^+\pi^-$ effic. ($\times 10^{-3}$)	$\Lambda_c^+\pi^-\pi^+\pi^-$ effic. ($\times 10^{-4}$)
$\Lambda_b^0 \to \Lambda_c(2593)^+\pi^-$	4.02±0.02	10.30±0.10	60.30±0.80
$\Lambda_b^0 \to \Lambda_c(2593)^+K^-$	3.97±0.02	10.50±0.10	62.80±0.80
$\Lambda_b^0 \to \Lambda_c(2625)^+\pi^-$	3.91±0.02	10.10±0.10	52.50±0.70
$\Lambda_b^0 \to \Lambda_c(2625)^+K^-$	3.87±0.02	10.30±0.10	54.60±0.70
$\Lambda_b^0 \to \Sigma_c(2455)^{++}\pi^-\pi^-$	2.50±0.02	3.09±0.06	31.50±0.60
$\Lambda_b^0 \to \Sigma_c(2455)^{++}\pi^-K^-$	2.37±0.02	2.28±0.05	32.40±0.60
$\Lambda_b^0 \to \Sigma_c(2455)^0\pi^-\pi^+$	2.67±0.02	1.64±0.04	6.10±0.20
$\Lambda_b^0 \to \Sigma_c(2455)^0K^-\pi^+$	2.69±0.02	1.66±0.04	6.50±0.30
$\Lambda_b^0 \to \Lambda_c^+\rho^0\pi^-$	2.15±0.01	1.11±0.03	10.80±0.30
$\Lambda_b^0 \to \Lambda_c^+\rho^0K^-$	2.07±0.01	0.73±0.03	11.00±0.30
$\Lambda_b^0 \to \Lambda_c^+\pi^-\pi^+\pi^-$	2.03±0.02	0.68±0.05	7.30±0.50
$\Lambda_b^0 \to \Lambda_c^+\pi^-\pi^+K^-$	1.86±0.01	0.44±0.02	8.40±0.30
$\Lambda_b^0 \to \Lambda_c^+\pi^-$	5.47±0.02	14.94±0.12	0
$\Lambda_b^0 \to \Lambda_c^+K^-$	5.45±0.02	14.97±0.12	0

Table C.4: *MC efficiency after trigger (TTT) and analysis cuts.*

(dashed blue line) and $\Lambda_c^+K^-$ (continuous red line), the invariant mass spectra in the mass hypothesis of $\Lambda_c^+\pi^-$ after the trigger and $\Lambda_c^+\pi^-$ selection. From the plots reported in these figures we count, for each decay mode, the number of CF and CS passing events. Finally in Fig. C.7, Fig. C.8 and Fig. C.9 we made, in logarithmic scale, the same plots of Fig. C.4, Fig. C.5 and Fig. C.6 normalizing each CS decay mode spectrum to the number of expected CS events (N^i_{CS}).

decay mode	(#*events CF*)	(#*events CS*)	(#*events CS exp.*)	N^i_{CS}/N^i_{CF}
$\Lambda_b^0 \to \Lambda_c^*(2595)^+$	6028	6281	526.60	0.087
$\Lambda_b^0 \to \Lambda_c^*(2625)^+$	5254	5456	300.74	0.057
$\Lambda_b^0 \to \Sigma_c(2455)^{++}$	3145	3241	281.92	0.089
$\Lambda_b^0 \to \Sigma_c(2455)^0$	614	654	36.80	0.060
$\Lambda_b^0 \to \Lambda_c^+\rho^0$	1075	1102	56.31	0.052
$\Lambda_b^0 \to \Lambda_c^+3\pi$	241	839	12.36	0.051
$\Lambda_b^0 \to \Lambda_c^+\pi$	14936	14965	805.16	0.054

Table C.5: *For each decay mode is reported the number of passing events for CF (#events CF = N^i_{CF}) and for CS (#events CS), the number of the expected CS events (#events CS exp. = N^i_{CS}) and the ratio N^i_{CS}/N^i_{CF} (scaling factor).*

The method described can be used to estimate the $\mathcal{B}(\Lambda_b^0 \to CS_i)/\mathcal{B}(\Lambda_b^0 \to CF_i)$ for the decay modes of Tab. C.1 using the corresponding B-mesons decays (see second column of Tab. C.6), and to estimate, for the same decay modes, the ratio of the MC efficiencies $\varepsilon^i_{CF}/\varepsilon^i_{CF}$. In the example illustrated here, we used a generator level MC and the resulting relative efficiencies are reported in the fourth column of Tab. C.6, while N^i_{CS}/N^i_{CF} is reported in the fifth column of the same Table. In the analysis this method was used to evaluate the systematic due to the CS yields in the Λ_b^0 mass window (see Sec. 7.1.1), using a fully simulated samples of 10^6 events for CS and CF decay mode of Tab. C.1. The CS events for each decay mode were normalized to the $10^6 \times \mathcal{B}(\Lambda_b^0 \to CS_i)/\mathcal{B}(\Lambda_b^0 \to CF_i)$. The fraction N^i_{CS}/N^i_{CF} after the trigger and the analysis cuts falling in the Λ_b^0 mass window of the ΔM^{--+} distribution was estimated counting the corresponding passing events, we call this fraction scaling factor. The systematic due to the CS background for each decay mode was then evaluated as the signal yield times this fraction.

Λ_b^0 decay mode	$R_i = \mathcal{B}_i/\mathcal{B}_0$	$\varepsilon_{analysis}$	$\varepsilon_i/\varepsilon_0$	$\Pi\ R_i(\varepsilon_i/\varepsilon_0)$
$\Lambda_b^0 \to \Lambda_c(2595)^+\pi^-$	1	$(2.42 \pm 0.09)\,10^{-4}$	1	1
$\Lambda_b^0 \to \Lambda_c(2595)^+K^-$	$(7.75 \pm 0.68)\,10^{-2}$	$(2.49 \pm 0.09)\,10^{-4}$	(1.03 ± 0.05)	$(7.98 \pm 1.09)\,10^{-2}$
$\Lambda_b^0 \to \Lambda_c(2625)^+\pi^-$	1	$(2.05 \pm 0.08)\,10^{-4}$	1	1
$\Lambda_b^0 \to \Lambda_c(2625)^+K^-$	$(5.55 \pm 0.28)\,10^{-2}$ [1]	$(2.11 \pm 0.08)\,10^{-4}$	(1.03 ± 0.05)	$(5.72 \pm 0.57)\,10^{-2}$
$\Lambda_b^0 \to \Sigma_c(2455)^{++}\pi^-\pi^-$	1	$(0.79 \pm 0.05)\,10^{-4}$	1	1
$\Lambda_b^0 \to \Sigma_c(2455)^{++}\pi^-K^-$	$(8.29 \pm 4.13)\,10^{-2}$	$(0.77 \pm 0.05)\,10^{-4}$	(0.97 ± 0.09)	$(8.04 \pm 4.75)\,10^{-2}$
$\Lambda_b^0 \to \Sigma_c(2455)^0\pi^+\pi^-$	1	$(0.16 \pm 0.05)\,10^{-4}$	1	1
$\Lambda_b^0 \to \Sigma_c(2455)^0\pi^+K^-$	$(5.40 \pm 3.26)\,10^{-2}$	$(0.17 \pm 0.05)\,10^{-4}$	(1.06 ± 0.46)	$(5.72 \pm 5.93)\,10^{-2}$
$\Lambda_b^0 \to \Lambda_c^+\rho^0\pi^-$	1	$(0.23 \pm 0.02)\,10^{-4}$	1	1
$\Lambda_b^0 \to \Lambda_c^+\rho^0K^-$	$(5.36 \pm 6.98)\,10^{-2}$	$(0.23 \pm 0.02)\,10^{-4}$	(1.00 ± 0.12)	$(5.36 \pm 7.62)\,10^{-2}$
$\Lambda_b^0 \to \Lambda_c^+\pi^-\pi^+\pi^-$	1	$(0.15 \pm 0.04)\,10^{-4}$	1	1
$\Lambda_b^0 \to \Lambda_c^+\pi^-\pi^+K^-$	$(5.42 \pm 2.11)\,10^{-2}$	$(0.16 \pm 0.02)\,10^{-4}$	(1.00 ± 0.02)	$(5.42 \pm 2.22)\,10^{-2}$
$\Lambda_b^0 \to \Lambda_c^+\pi^-$	1	$(8.17 \pm 0.13)\,10^{-4}$	1	1
$\Lambda_b^0 \to \Lambda_c^+K^-$	$(7.66 \pm 1.18)\,10^{-2}$	$(8.16 \pm 0.13)\,10^{-4}$	(0.99 ± 0.02)	$(7.58 \pm 1.32)\,10^{-2}$

Table C.6: *This summary reports, for each Λ_b^0 decay modes, the relative $\mathcal{B}$, the analysis efficiency, the relative efficiencies, and the product of $\Pi\ R_i(\varepsilon_i/\varepsilon_0)$, which for the i^{th} decay mode is the evaluated N^i_{CS}/N^i_{CF} (scaling factor for the i^{th} decay mode).*

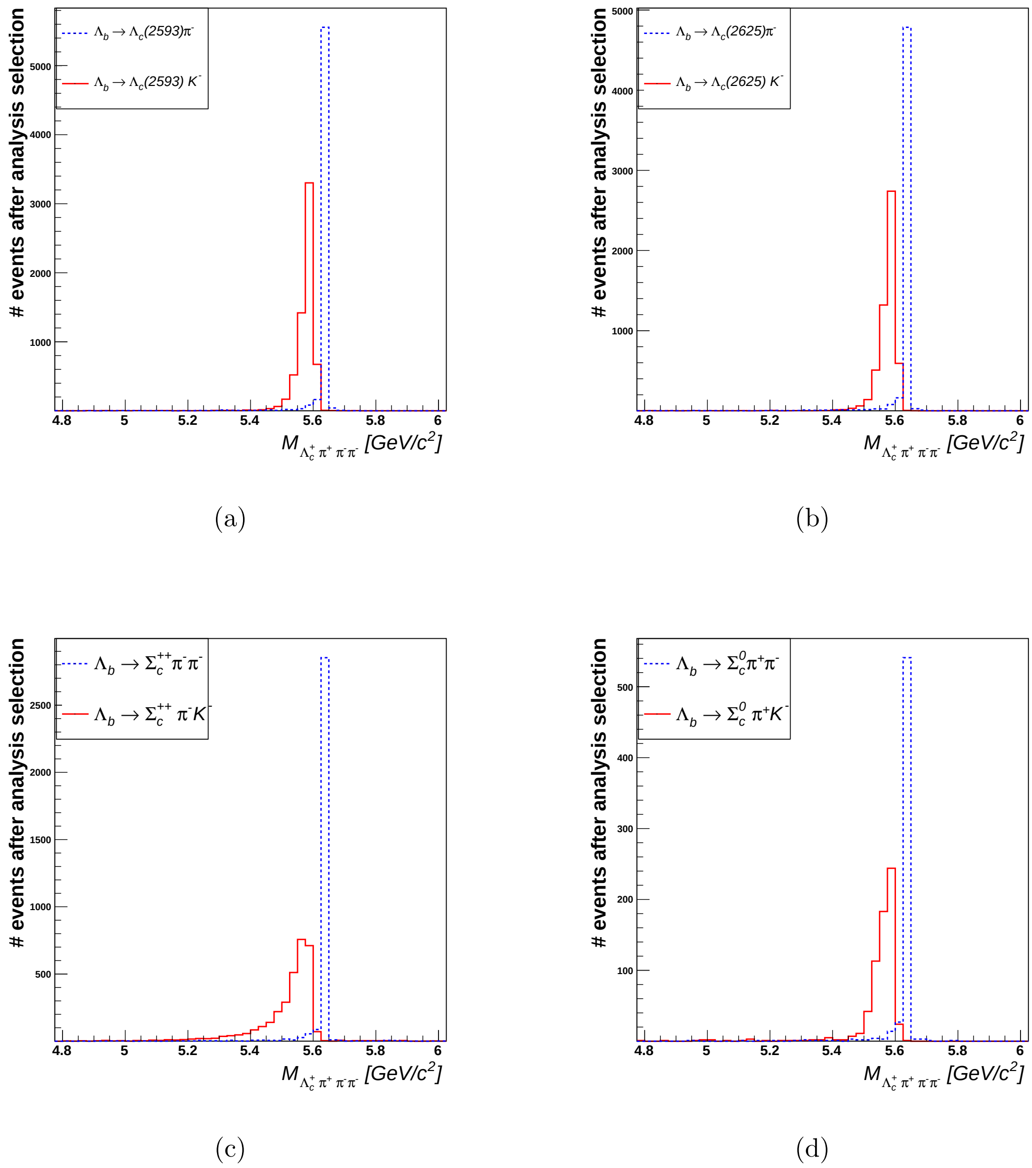

Figure C.4: *$\Lambda_c^+\pi^-\pi^+\pi^-$ invariant mass spectra for $\Lambda_b^0 \to \Lambda_c^+(2595)^+\pi^-$ and $\Lambda_b^0 \to \Lambda_c^+(2595)^+K^-$* **C.4(a)**, *$\Lambda_b^0 \to \Lambda_c^+(2625)^+\pi^-$ and $\Lambda_b^0 \to \Lambda_c^+(2625)^+K^-$* **C.4(b)**, *$\Lambda_b^0 \to \Sigma_c(2455)^{++}\pi^-\pi^-$ and $\Lambda_b^0 \to \Sigma_c(2455)^{++}\pi^-K^-$* **C.4(c)** *and $\Lambda_b^0 \to \Sigma_c(2455)^0\pi^+\pi^-$ and $\Lambda_b^0 \to \Sigma_c(2455)^0\pi^+K^-$* **C.4(d)** *resonant final states after the trigger and $\Lambda_c^+\pi^-\pi^+\pi^-$ selection.*

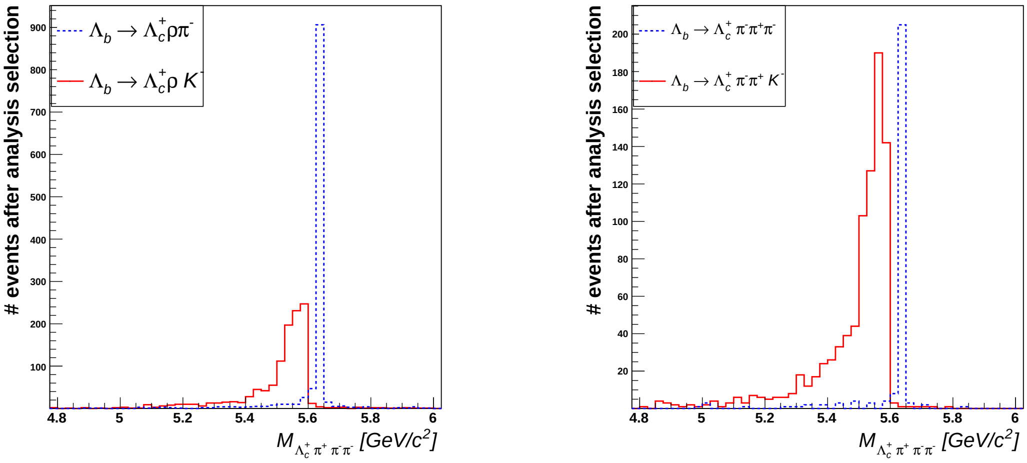

(a) (b)

Figure C.5: $\Lambda_c^+\pi^-\pi^+\pi^-$ *invariant mass spectra for* $\Lambda_b^0 \to \Lambda_c^+\rho^0\pi^-$ *and* $\Lambda_b^0 \to \Lambda_c^+\rho^0 K^-$ **C.5(a)** *and* $\Lambda_b^0 \to \Lambda_c^+\pi^-\pi^+\pi^-$ *and* $\Lambda_b^0 \to \Lambda_c^+\pi^-\pi^+K^-$ **C.5(b)** *resonant final states after the trigger and* $\Lambda_c^+\pi^-\pi^+\pi^-$ *selection: the dashed line and the continuous one indicate the invariant mass distribution of the corresponding CF and CS decay modes reported in Tab. C.4.*

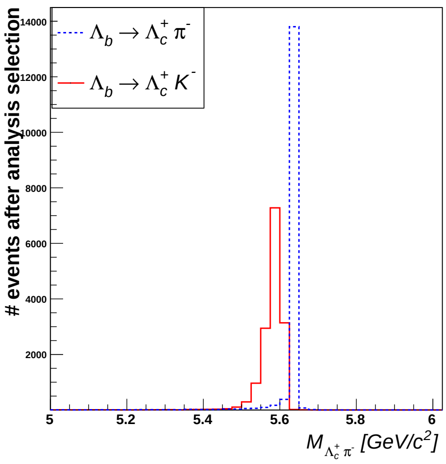

Figure C.6: $\Lambda_c^+\pi^-$ *invariant mass for the decay mode* $\Lambda_b^0 \to \Lambda_c^+\pi$ *(Tab. C.4) after the trigger and* $\Lambda_c^+\pi$ *requirements. The dashed line and the continuous one indicate the invariant mass distribution of the corresponding CF and CS decay modes.*

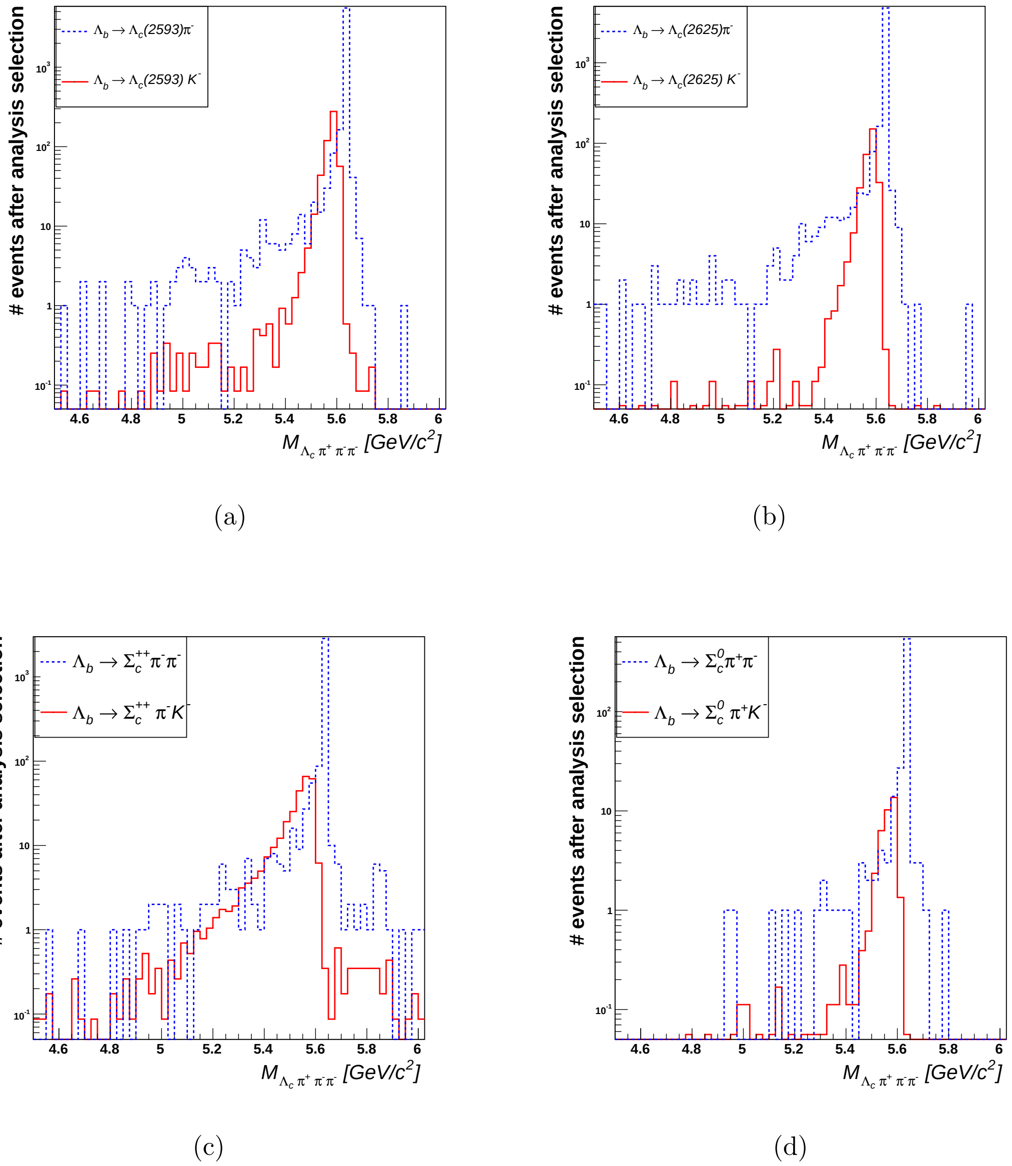

Figure C.7: *$\Lambda_c^+\pi^-\pi^+\pi^-$ invariant mass spectra for $\Lambda_b^0 \to \Lambda_c^+(2595)^+\pi^-$ and $\Lambda_b^0 \to \Lambda_c^+(2595)^+K^-$* **C.7(a)**, *$\Lambda_b^0 \to \Lambda_c^+(2625)^+\pi^-$ and $\Lambda_b^0 \to \Lambda_c^+(2625)^+K^-$* **C.7(b)**, *$\Lambda_b^0 \to \Sigma_c(2455)^{++}\pi^-\pi^-$ and $\Lambda_b^0 \to \Sigma_c(2455)^{++}\pi^-K^-$* **C.7(c)** *and $\Lambda_b^0 \to \Sigma_c(2455)^0\pi^+\pi^-$ and $\Lambda_b^0 \to \Sigma_c(2455)^0\pi^+K^-$* **C.7(d)** *resonant final states after trigger and Λ_c^+ 3π selection.*

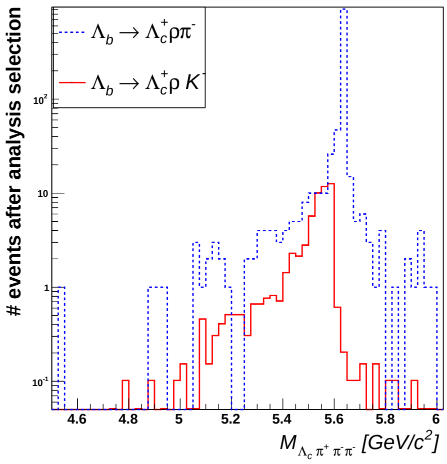

(a)

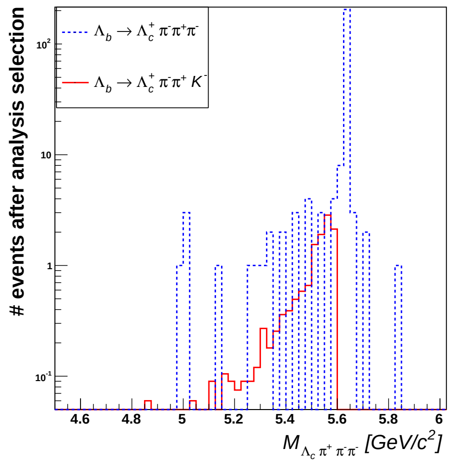

(b)

Figure C.8: $\Lambda_c^+\pi^-\pi^+\pi^-$ *invariant mass spectra for* $\Lambda_b^0 \to \Lambda_c^+\rho^0\pi^-$ *and* $\Lambda_b^0 \to \Lambda_c^+\rho^0 K^-$ **C.8(a)** *and* $\Lambda_b^0 \to \Lambda_c^+\pi^-\pi^+\pi^-$ *and* $\Lambda_b^0 \to \Lambda_c^+\pi^-\pi^+K^-$ **C.8(b)** *resonant final states after trigger and* Λ_c^+ 3π *selection: the dashed line and the continuous one indicate the invariant mass distribution of the corresponding CF and CS decay modes that are reported in Tab. C.4.*

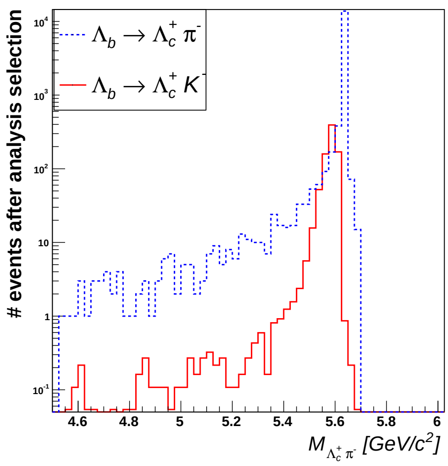

Figure C.9: $\Lambda_c^+\pi^-$ *invariant mass for the decay* $\Lambda_b^0 \to \Lambda_c^+\pi$ *in Tab. C.4 after the trigger and* $\Lambda_c^+\pi^-$ *selection. The dashed line indicate the invariant mass distribution of the corresponding CF decay.*

Appendix D

Study of $\Lambda_b^0 \to \Lambda_c^+ \pi^- \pi^+ \pi^-$ without Charmed Resonant Decay Modes

Here we investigate on the composition of the $\Lambda_b^0 \to \Lambda_c^+ \pi^- \pi^+ \pi^-$ signal, after the veto on the Λ_b^0 charmed resonant decay modes. This study was done after the the analysis presented in this Thesis was officially approved by the Collaboration.

D.1 Motivations

In Chap. 6 we assumed proportions (1/2, 1/2, 0) or (1/2, 0, 1/2) respectively of $\Lambda_b^0 \to \Lambda_c^+ \rho^0 \pi^- \to \Lambda_c^+ \pi^- \pi^+ \pi^-$, $\Lambda_b^0 \to \Lambda_c^+ \pi^- \pi^+ \pi^- (nr)$ and $\Lambda_b^0 \to \Lambda_c^+ a_1(1260)^- \to \Lambda_c^+ \rho^0 \pi^- \to \Lambda_c^+ \pi^- \pi^+ \pi^-$ contributing to the mixed E, since, we declared, we were not able to separate the contributions of these states, and to extract their yields. The proportions assumed are importants since determine how to evaluate the efficiency of the mixed E state. As example, when assumed proportions are (1/2, 1/2, 0), the efficiency of the mixed E state is the average of the efficiencies of $\Lambda_b^0 \to \Lambda_c^+ \rho^0 \pi^- \to \Lambda_c^+ \pi^- \pi^+ \pi^-$ (F state) and of $\Lambda_b^0 \to \Lambda_c^+ \pi^- \pi^+ \pi^- (nr)$ (G state), since we can write:

$$\frac{N(E)^{prod}}{2} = N(F)^{prod} = \frac{N(F)^{obs}}{\varepsilon_F} \tag{D.1}$$

$$\frac{N(E)^{prod}}{2} = N(G)^{prod} = \frac{N(G)^{obs}}{\varepsilon_G} \tag{D.2}$$

$$\frac{N(F)^{obs} + N(G)^{obs}}{N(E)^{prod}} = \frac{\varepsilon_F + \varepsilon_G}{2} \tag{D.3}$$

Where $N(E)$, $N(F)$ and $N(G)$ indicate the number of events of the three states, and ε_F and ε_G are the MC efficiencies of the states F and G.

It is evident that it is important to know the decay modes which really contribute to $\Lambda_b^0 \rightarrow \Lambda_c^+\pi^-\pi^+\pi^-(nr)$ after the veto on the Λ_b^0 charmed resonant decay modes, as well as to measure theirs yields, since one of the dominant systematic in the measurement of the relative branching fractions, reported in Tab. 6.4 and Tab. 6.5, arises from the assumption of the unknown proportions. In the following we decribe the studies done to investigate on the composition of the $\Lambda_b^0 \rightarrow \Lambda_c^+\pi^-\pi^+\pi^-$ signal, after the veto on the Λ_b^0 charmed resonant decay modes.

D.2 ρ^0 Signal Contribution to the $\Lambda_b^0 \rightarrow \Lambda_c^+\pi^-\pi^+\pi^-$ Decay after the Veto on Charmed Resonant Decay Modes.

In Fig. 5.10(b) we reported the ΔM^{--+} distribution obtained after the veto on the Λ_b^0 charmed resonant decay modes (see Chap. 5) with overlaid the best fit results when assuming in the modeling a Gaussian function for the signal, an exponential for the combinatorial background, and including the $\overline{B}^0_{(s)} \rightarrow D^{(*)+}_{(s)}\pi^-\pi^+\pi^-$, with inclusive $D^{(*)+}_{(s)}$ and $\overline{B}^0_{(s)}$ contributions, for the physics background.

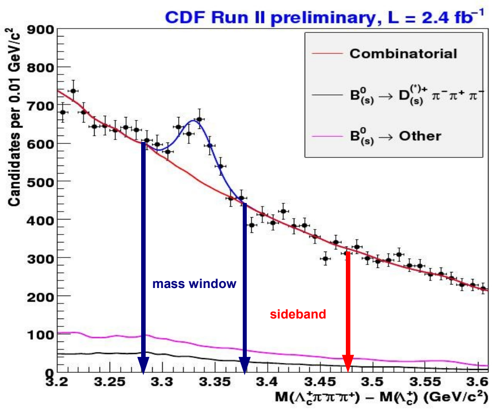

Figure D.1: *ΔM^{--+} distribution with indicated the mass window (MW) and the sideband (SB) used in the text.*

The resulting Gaussian mean and σ (sig_gauss_M in the legenda of Fig. 5.10(b)) from the best fit are used to define the $\Delta M^{--+} \pm 3\sigma$ mass window region (MW=$\Delta M^{--+}\pm 3\sigma = 3.332\pm 0.048$ GeV$/c^2$) and the sideband region (SB=$[\Delta M^{--+} + 3\sigma, \Delta M^{--+} + 6\sigma]$) as shown in Fig. D.1. Useful quantities, determined using the best fits and that will be used in the next section, are reported in Tab. D.1.

total events in MW	5515
total events in SB	$\mathsf{SB}_{sb} = 3559$
signal events in MW	610 ± 88 (`sig_n` in the legenda of Fig. 5.10(b))
background events in MW	MW_{bkg} = 5515-610 = 4905
sideband normalization	$\frac{\mathsf{MW}_{bkg}}{\mathsf{SB}_{sb}} = \frac{4905}{3559} = 1.38$

Table D.1: *Some useful quantities determined using the best fit parameters of the ΔM^{--+} distribution of Fig. 5.10(b).*

To demonstrate a ρ^0 signal in the Λ_b^0 mass window of Fig. D.1, we reconstruted, for each Λ_b^0 candidate in MW and in SB, the ρ^0 candidates using a pair of tracks of opposit sign, not from the Λ_c^+, assigning both the pion mass. For each Λ_b^0 candidate, the six tracks from the $\Lambda_b^0 \to \Lambda_c^+\pi^-\pi^+\pi^-$ decay mode are ordered in this way:

$$\underbrace{\overbrace{K^-}^{1}\ \overbrace{p}^{2}\ \overbrace{\pi^+}^{3}}_{\Lambda_c^+}\ \overbrace{\pi^-}^{4}\ \overbrace{\pi^-}^{5}\ \overbrace{\pi^+}^{6}$$

The same sign *pions* are ordered by momentum, and it means that $p_4 > p_5$.
The main difficulty is given by the fact that we are dealing with these two possible ρ^0 candidates: one with an high p_T (the ρ^0_{high} combination, using tracks 4 and 6) and the other one with a low p_T (the ρ^0_{low} combination, using tracks 5 and 6). Fig. D.2(a) shows the distribution of the invariant mass spectrum of the two pions forming the ρ^0_{high} candidates when the Λ_b^0 candidate is in the MW (red filled histogram) with overlaid the same distribution when the Λ_b^0 candidate is in the SB region (yellow filled histrogram, normalized to the background content of Fig. 5.10(b), see Tab. D.1, for the sideband normalization), while Fig. D.2(b) shows the same distributions but for the ρ^0_{low} candidates.
The two pion combinations have different invariant mass spectra ($M_{\rho^0_{high}}$ and $M_{\rho^0_{low}}$) both in MW and SB regions (see Fig. D.2(a) and Fig. D.2(b)), but in Fig. D.2(b) it is evident a clear signal of the ρ^0 resonance (ρ^0 Mass $= (775.49 \pm 0.34)$MeV, Full width Γ=(149.1 ± 0.8)MeV [1]).

In the following we describe some of the techniques tested to extract the contributions from the $\Lambda_b^0 \to \Lambda_c^+\rho^0\pi^- \to \Lambda_c^+\pi^-\pi^+\pi^-$, $\Lambda_b^0 \to \Lambda_c^+a_1(1260)^- \to \Lambda_c^+\rho^0\pi^- \to \Lambda_c^+\pi^-\pi^+\pi^-$ and the non-resonant $\Lambda_b^0 \to \Lambda_c^+\pi^-\pi^+\pi^-(nr)$ to the $\Lambda_b^0 \to \Lambda_c^+\pi^-\pi^+\pi^-$ without charmed resonances.

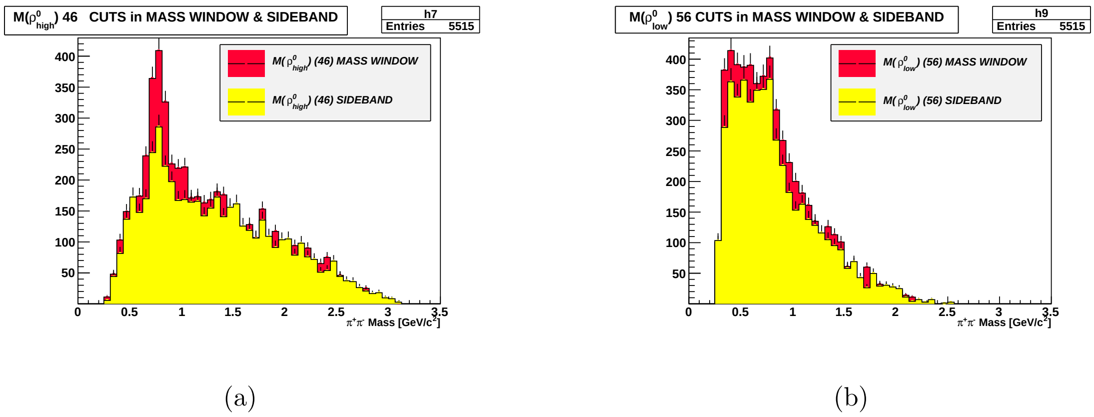

Figure D.2: *$M_{\rho^0_{high}}$ **D.2(a)** and $M_{\rho^0_{low}}$ **D.2(b)** $\pi^+\pi^-$ invariant mass distribution in the mass window (red filled histogram) and in the sideband (yellow filled histogram) after vetoed the Λ_b^0 charmed resonant decay modes.*

D.2.1 Estimate of the yields for the decay modes with a ρ^0 and the $\Lambda_b^0 \to \Lambda_c^+\pi^-\pi^+\pi^-(nr)$

We want now extract the signal yields of the sum of the $\Lambda_b^0 \to \Lambda_c^+\rho^0\pi^- \to \Lambda_c^+\pi^-\pi^+\pi^-$ and of the $\Lambda_b^0 \to \Lambda_c^+ a_1(1260)^- \to \Lambda_c^+\rho^0\pi^- \to \Lambda_c^+\pi^-\pi^+\pi^-$, and of the $\Lambda_b^0 \to \Lambda_c^+\pi^-\pi^+\pi^-(nr)$.

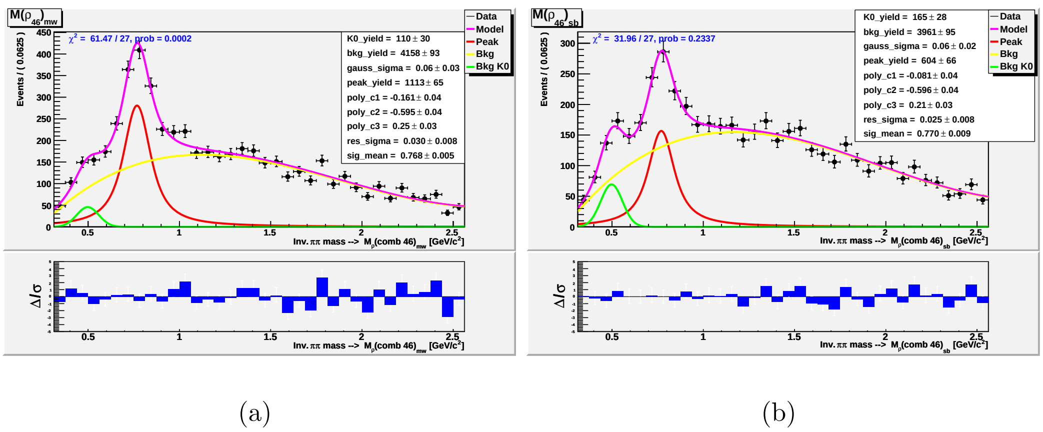

Figure D.3: *$M_{\rho^0_{high}}$ mass distribution with overlaid the best fit curve (magenta curve) in the mass window **D.3(a)** and in the sideband **D.3(b)** in range $[0.3 - 2.6]$ GeV/c^2.*

In order to that, we made a fit of both $M_{\rho^0_{high}}$ and $M_{\rho^0_{low}}$ mass distribution in both

MW and SB regions.
The fit is performed in the range $[0.3-2.6]$ GeV/c^2 using different PDFs to model the $M_{\rho^0_{high}}$ and $M_{\rho^0_{low}}$ in the MW and SB regions. The $M_{\rho^0_{high}}$ distribution is modeled, in MW and SB regions, with a PDF composed of: a Voigtian function for the ρ^0 signal, with a width fixed to the PDG value ($\Gamma_{\rho^0} = 0.149\,\text{GeV}$) and the mass resolution Gaussian with sigma and mean free to float in the fit, a Gaussian function with mean fixed to the central value of the K^0 mass ($M_{K^0} = 0.498\,\text{GeV}$ [1]) and the sigma free to float in the fit, and a third degree Chebyshev polynomial for the background.
The PDF function used to model the $M_{\rho^0_{low}}$ is parameterized like the $M_{\rho^0_{high}}$ one with the exception that we used a convolution between a Landau and an exponential function for the background.
In Fig. D.3 and Fig. D.4 we report the mass distribution fit in both MW and SB regions for the two possible combination ρ^0_{high} and ρ^0_{low}.
All have a signal of $\rho^0\pi^-\pi^+$, the ρ^0 mass returned by the best fits are in agreement with the measured ρ^0 mass (see variables `sig_mean` for the mass and the `res_sigma` for the uncertainty on it in the fit results legenda of these figures).
The parameters estimated from the fits in Fig. D.3(a) and Fig. D.3(b) are summarized on Tab. D.2, where the total ρ^0_{high} and ρ^0_{low} in the $\Lambda_b^0 \rightarrow \Lambda_c^+\pi^-\pi^+\pi^-$ signal is the difference between the ρ^0 signal yield fitted in the MW and the one fitted in the SB region, respectively for $M_{\rho^0_{high}}$ and $M_{\rho^0_{low}}$ combinations.

Yields of $\rho^0 \rightarrow \pi^-\pi^+$	
ρ^0_{high} in MW	1113 ± 65 (`peak_yield` in the legenda of Fig. D.3(a))
ρ^0_{high} in normalized SB	604 ± 66 (`peak_yield` in the legenda of Fig. D.3(b))
ρ^0_{high} in $\Lambda_b^0 \rightarrow \Lambda_c^+\pi^-\pi^+\pi^-$ signal	509 ± 93
ρ^0_{low} in MW	329 ± 64 (`peak_yield` in the legenda of Fig. D.4(a))
ρ^0_{low} in normalized SB	299 ± 71 (`peak_yield` in the legenda of Fig. D.4(b))
ρ^0_{low} in $\Lambda_b^0 \rightarrow \Lambda_c^+\pi^-\pi^+\pi^-$ signal	30 ± 96

Table D.2: *Yields of ρ^0_{high} and ρ^0_{low} in the MW and in the SB regions obtained from the best fit of $M_{\rho^0_{high}}$ and $M_{\rho^0_{low}}$ distributions reported in Fig. D.3(a) and Fig. D.3(b). The yield of the ρ^0_{high} (ρ^0_{low}) in the $\Lambda_b^0 \rightarrow \Lambda_c^+\pi^-\pi^+\pi^-$ is given by the difference between the yields ρ^0_{high} (ρ^0_{low}) in the MW and in the SB.*

In Tab. D.3 we report N_{TOT}, that is the resulting yield of the fit reported on Fig. 5.10(b), and the total yield of the ρ^0 (N_{ρ^0}), that in principle is due to the $\Lambda_b^0 \rightarrow \Lambda_c^+\rho^0\pi^- \rightarrow \pi^-\pi^+\pi^-$ and $\Lambda_b^0 \rightarrow \Lambda_c^+a_1(1260)^- \rightarrow \Lambda_c^+\rho^0\pi^- \rightarrow \pi^-\pi^+\pi^-$ decays,

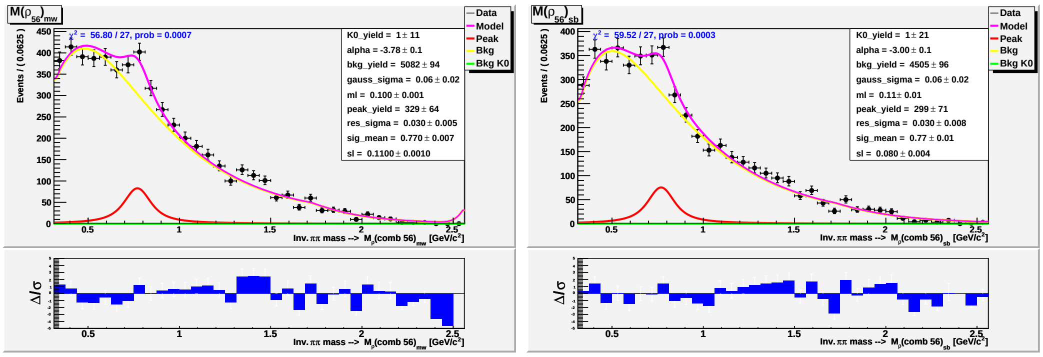

(a) (b)

Figure D.4: *$M_{\rho^0_{low}}$ mass distribution fit with overlaid the best fit curve (magenta curve) in the mass window* **D.4(a)** *and in the sideband* **D.4(b)** *in range* $[0.3 - 2.6]$ GeV/c^2.

calculated as the sum of ρ^0_{high} and ρ^0_{low} in $\Lambda_b^0 \to \Lambda_c^+\pi^-\pi^+\pi^-$ signal of Tab. D.2. In the same Table is reported the yield of the $\Lambda_b^0 \to \Lambda_c^+\pi^-\pi^+\pi^-(nr)$ (N_{nr}) calculated as the difference between the total number of Λ_b^0 signal yield, after the veto on the Λ_b^0 charmed resonant decay modes (N_{TOT}), and N_{ρ^0}. The quoted result for N_{nr} is consistent with the LHCb claim [17] which considers the proportion of $\Lambda_b^0 \to \Lambda_c^+\pi^-\pi^+\pi^-(nr)$ decay mode as null.

Λ_b^0 Decay Mode	Signal Yield
$N_{TOT} = N(\Lambda_b^0 \to \Lambda_c^+\rho^0\pi^- + N(\Lambda_b^0 \to \Lambda_c^+ a_1(1260)^-)_{obs}) + N(\Lambda_b^0 \to \Lambda_c^+\pi^-\pi^+\pi^-(nr))$	610 ± 88
$N_{\rho^0} = N(\Lambda_b^0 \to \Lambda_c^+\rho^0\pi^-)_{obs} + N(\Lambda_b^0 \to \Lambda_c^+ a_1(1260)^-)_{obs}$	539 ± 133
$N_{nr} = N(\Lambda_b^0 \to \Lambda_c^+\pi^-\pi^+\pi^-(nr))$	71 ± 159

Table D.3: *In this table we report the yield of the $\Lambda_b^0 \to \Lambda_c^+\pi^-\pi^+\pi^-$ after the veto on the charmed resonances (N_{TOT}), the yield of the ρ^0 (N_{ρ^0}) that in principle are due the $\Lambda_b^0 \to \Lambda_c^+\rho^0\pi^- \to \pi^-\pi^+\pi^-$ and $\Lambda_b^0 \to \Lambda_c^+ a_1(1260)^- \to \Lambda_c^+\rho^0\pi^- \to \pi^-\pi^+\pi^-$ decays, and the yield of the $\Lambda_b^0 \to \Lambda_c^+\pi^-\pi^+\pi^-(nr)$ (N_{nr}).*

D.3 *sPlot* to separate the contributions in $\Lambda_b^0 \to \Lambda_c^+\pi^-\pi^+\pi^-$

In these next Sections we want to use another technique to confirm, or improve, the results obtained in the previous one. The aim is to determine the composition of our $\Lambda_b^0 \to \Lambda_c^+\pi^-\pi^+\pi^-$ sample, after the veto on the charmed resonant decay modes, measuring the yields of the contributing decay modes: $\Lambda_b^0 \to \Lambda_c^+\rho^0\pi^-$, $\Lambda_b^0 \to \Lambda_c^+a_1(1260)^-$ and $\Lambda_b^0 \to \Lambda_c^+\pi^-\pi^+\pi^-(nr)$, all in $\Lambda_b^0 \to \Lambda_c^+\pi^-\pi^+\pi^-$ final state. In order to do that, we decided to use a statistical tool dedicated to the exploration of data samples populated by several classes of events, called *sPlot* [100], [101].
With the *sPlot* we can explore a data sample, consisting of several classes of events merged into a single sample, assumed to be characterized by a set of variables which can be split into two components: the first one is a set of variables for which the distributions of all the classes of events are known (these variables are collectively referred to as a (unique) *discriminating variable*). The second component is a set of variables for which the distributions of some classes of events are either truly unknown or considered as such (these variables are collectively referred to as a (unique) *control variable*).
The *sPlot* technique allows us to reconstruct the distributions for the control variable, independently for each of the various classes of events, without making use of any a priori knowledge on this variable with the assumption that the control variable is uncorrelated with the discriminating variable. The general idea is to use the *sPlot*, first of all, in the ΔM^{--+} mass distribution fit (see in Fig. 5.10(b)), where signal and background events can be separated by one-dimensional likelihood fit, in order to obtain the two respective yields. Then, this technique uses the results from the ΔM^{--+} fit to calculate a weight (termed SWeights) for each event, i.e. a sort of *signal-likeness/background-likeness* of a specific event, in order to obtain a *weighted dataset*. With the specific weights, the mass distribution of two pions can also be separated into the event classes, much better than an advanced sideband subtraction because this is an unbinned subtraction between signal and background, and the weighted dataset is being the result.
After having obtained the weighted dataset, we projected on it the variables that represent the mass distribution of two pions (ρ^0_{high} and ρ^0_{low}). We did the same with the invariant mass of three pions, $m3\pi$, not from Λ_c^+ (tracks 4, 5, 6 of Sec. D.2) to investigate on the $a_1(1260)^- \to \rho^0\pi^- \to \pi^-\pi^+\pi^-$ signal.
The projections for these three control variables ρ^0_{high}, ρ^0_{low} and $m3\pi$ on the weighted dataset are reported in Fig. D.5.

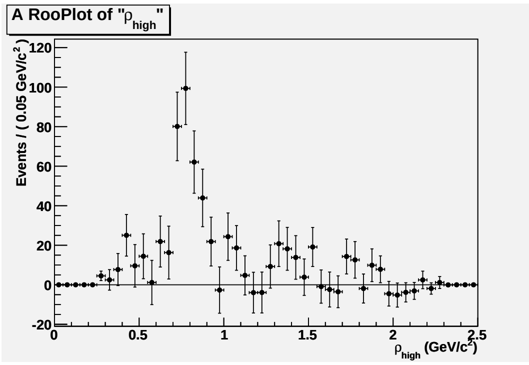

(a)

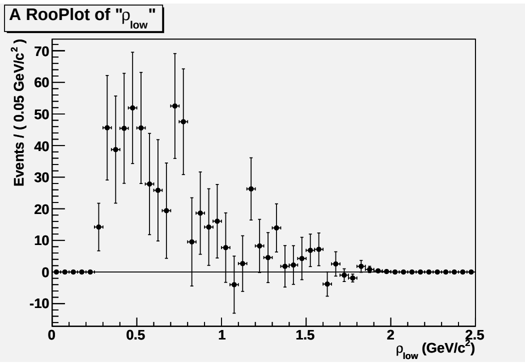

(b)

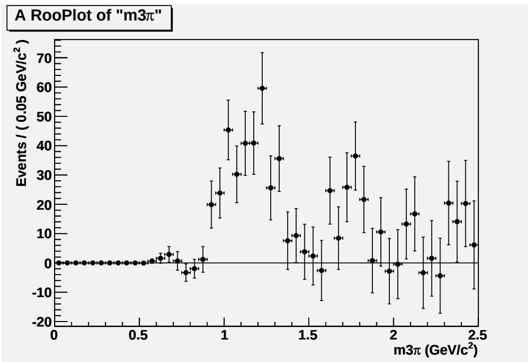

(c)

Figure D.5: *ρ^0_{high}* **D.5(a)***, ρ^0_{low}* **D.5(b)** *and $m3\pi$* **D.5(c)** *invariant mass projections on the weighted dataset.*

Fig. D.5(a) shows a clear ρ^0 peak and Fig. D.5(c) also shows peak due to the $a_1(1260)^-$ ($a_1(1260)^-$ Full width Γ from 250 to 600 MeV [1]), confirming the contribution of the $\Lambda_b^0 \to \Lambda_c^+ a_1(1260)^- \to \Lambda_c^+\rho^0\pi^- \to \Lambda_c^+\pi^-\pi^+\pi^-$ in the Λ_b^0 signal, after the veto on the charmed resonant decay modes.
At this point, once obtained the projections on the weighed dataset, the next step is to find a way to fit these distributions, in order to obtain the yields in the hypothesis that the decay modes contributing to the $\Lambda_b^0 \to \Lambda_c^+\pi^-\pi^+\pi^-$ signal after the veto on the charmed resonances are: $\Lambda_b^0 \to \Lambda_c^+\rho^0\pi^- \to \Lambda_c^+\pi^-\pi^+\pi^-$, $\Lambda_b^0 \to \Lambda_c^+\pi^-\pi^+\pi^-(nr)$ and $\Lambda_b^0 \to \Lambda_c^+ a_1(1260)^- \to \Lambda_c^+\rho^0\pi^- \to \Lambda_c^+\pi^-\pi^+\pi^-$.
First of all, as a cross check of the ρ^0 yield determined in Sec. D.2, we performed a fit of the projections of the two control variables ρ^0_{high} and ρ^0_{low} on the weighted dataset of Fig. D.5(a) and Fig. D.5(b) using MC templates of these distributions

for the three decay modes.
The fact that in principle there can be two different combinations of a pion pair, is a reason to make the fit of one of the two combinations (ρ^0_{high}, having the best mass resolution) and to use the achieved results in terms of composition as a cross-check on the other one. In the next Sections we illustrate the method to determine the templates of the three decay modes using MC samples and the fit procedure adopted to separate these contributions in the data.

D.3.1 Templates Extraction from MC

The main difficulty to separate the three decay modes concerns the separation of the $\Lambda_b^0 \to \Lambda_c^+\rho^0\pi^-$ from $\Lambda_b^0 \to \Lambda_c^+ a_1(1260)^-$ candidates, since $a_1(1260)^- \to \rho^0\pi^-$. In order to make the fit on the weighted dataset of the ρ^0_{high} and ρ^0_{low} distributions we construct MC templates (shapes) of these distributions from the three decay modes, that we describe in the following.
We generated MC samples of $\approx\ \times 10^6$ events for the $\Lambda_b^0 \to \Lambda_c^+ a_1(1260)^- \to \Lambda_c^+\rho^0\pi^- \to \Lambda_c^+\pi^-\pi^+\pi^-$, $\Lambda_b^0 \to \Lambda_c^+\rho^0\pi^- \to \Lambda_c^+\pi^-\pi^+\pi^-$, and $\Lambda_b^0 \to \Lambda_c^+\pi^-\pi^+\pi^-(nr)$ decay modes and reconstructed, like on data, ρ^0_{high} and ρ^0_{low} candidates in the Λ_b^0 mass window.
For each MC sample, corresponding to one of the three decay modes, we have two possible combinations, ρ^0_{high} and ρ^0_{low}, the first one using the tracks 4 and 6 (see Sec. D.2) and the second one using the tracks 5 and 6, and for each of them we fill two different kind of histograms that we call *good histogram* and *bad histogram*.
The *good histogram* is filled for the track pair 5 and 6 with the invariant mass of the reconstructed ρ^0_{low} candidate when the corresponding two pions are from the ρ^0 decay, while, when the pion pair is not from the ρ^0 decay, the *bad histogram* is filled with ρ^0_{low} candidate reconstructed mass. The same is done for the *good histogram* and *bad histogram* for the 4 and 6 tracks combination.
The ρ^0_{high} invariant mass spectrum for the weighted data sample is expected to have contributions from:

- $\Lambda_b^0 \to \Lambda_c^+\rho^0\pi^-$ decay mode, when the track pair is from the ρ^0 decay (Fig. D.6 top histogram reports the invariant mass distribution for the true track pair 4 and 6) and when the track pair is the wrong one (Fig. D.6 bottom histogram reports the invariant mass distribution for the wrong track pair 4 and 6).

- $\Lambda_b^0 \to \Lambda_c^+ a_1(1260)^- \to \Lambda_c^+\rho^0\pi^-$ decay mode, when the track pair is from the ρ^0 decay (Fig. D.8 top histogram reports the invariant mass distribution for the true track pair 4 and 6) and when the track pair is the wrong one (Fig. D.8, bottom histogram report the invariant mass distribution for the wrong track pair 4 and 6).

- $\Lambda_b^0 \to \Lambda_c^+\pi^-\pi^+\pi^-(nr)$, in this case the track pair is wrong in any case, (Fig. D.10, top histogram reports the invariant mass distribution for the track pair 4 and 6).

The corresponding distributions contributing to the ρ^0_{low} invariant mass spectrum are reported in Fig. D.7 (top histogram good combination, bottom histogram wrong combination for the $\Lambda_b^0 \to \Lambda_c^+\rho^0\pi^-$), Fig. D.9 (top histogram good combination, bottom histogram wrong combination for the $\Lambda_b^0 \to \Lambda_c^+ a_1(1260)^- \to \Lambda_c^+\rho^0\pi^-$) and in the bottom of Fig. D.10 (for the $\Lambda_b^0 \to \Lambda_c^+\pi^-\pi^+\pi^-(nr)$). For each decay mode, each pair of the invariant mass distibution of Fig. D.6, Fig. D.7, Fig. D.8, Fig. D.9, are fitted separately and then merged togheter to obtain the templates for the ρ^0_{high} and ρ^0_{low} mass distributions for the contribution mentioned above.
We could have used directly the distributions of ρ^0_{low} and ρ^0_{high} as reconstructed in the MC for each decay mode, but since the shapes of good and bad histograms are very different, this procedure guarantees a better description of them.
For the two pions contribution from $\Lambda_b^0 \to \Lambda_c^+\pi^-\pi^+\pi^-(nr)$, the templates for ρ^0_{high} and ρ^0_{low} are respectively obtained fitting the invariant mass distribution of Fig. D.10 top histogram and Fig. D.10 bottom histogram. Fig. D.11 shows the templates of the three decay modes normalized to the unit (PDFs) for the ρ^0_{high} (Fig. D.11(a)) and for the ρ^0_{low} (Fig. D.11(b)).

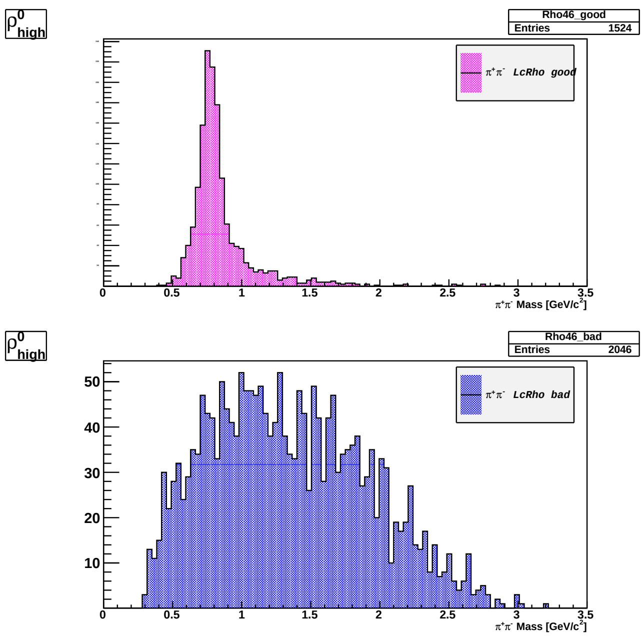

Figure D.6: *MC contributions to ρ^0_{high} from $\Lambda_b^0 \to \Lambda_c^+\rho^0\pi^-$ decay.*

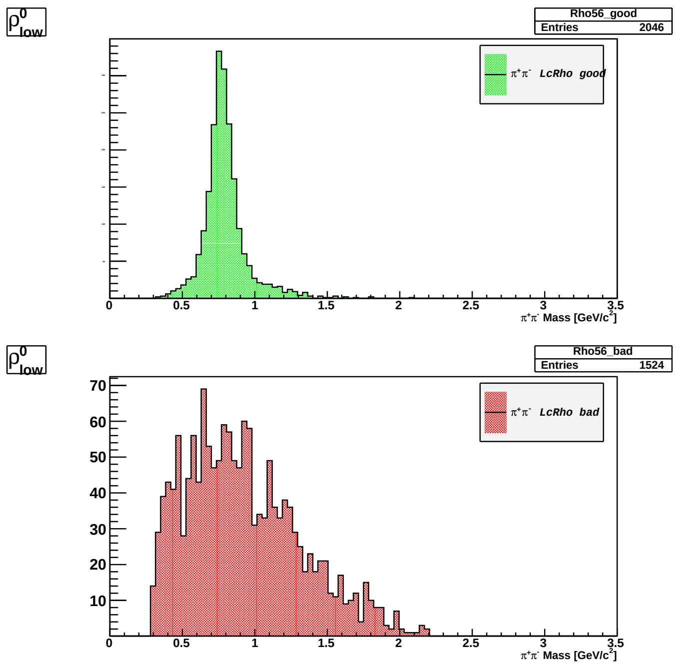

Figure D.7: *MC contributions to ρ^0_{low} from $\Lambda_b^0 \to \Lambda_c^+\rho^0\pi^-$ decay.*

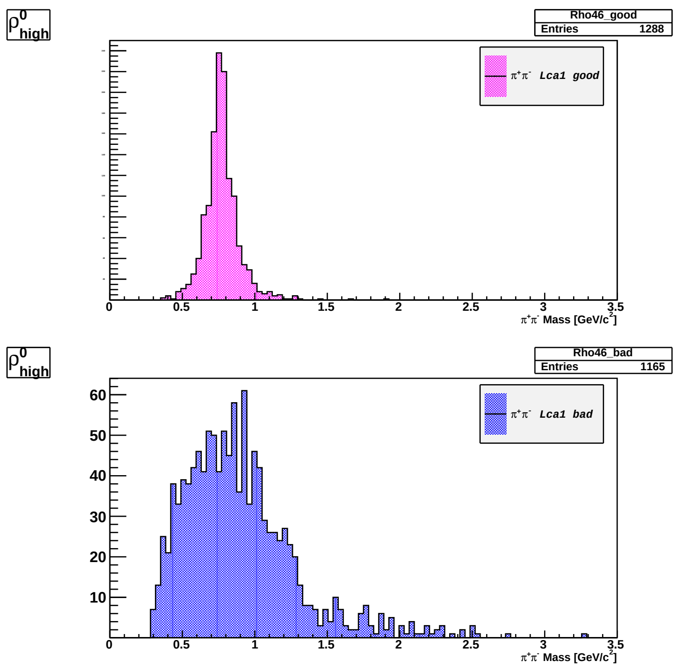

Figure D.8: *MC contributions to ρ^0_{high} from $\Lambda_b^0 \to \Lambda_c^+ a_1(1260)^-$ decay.*

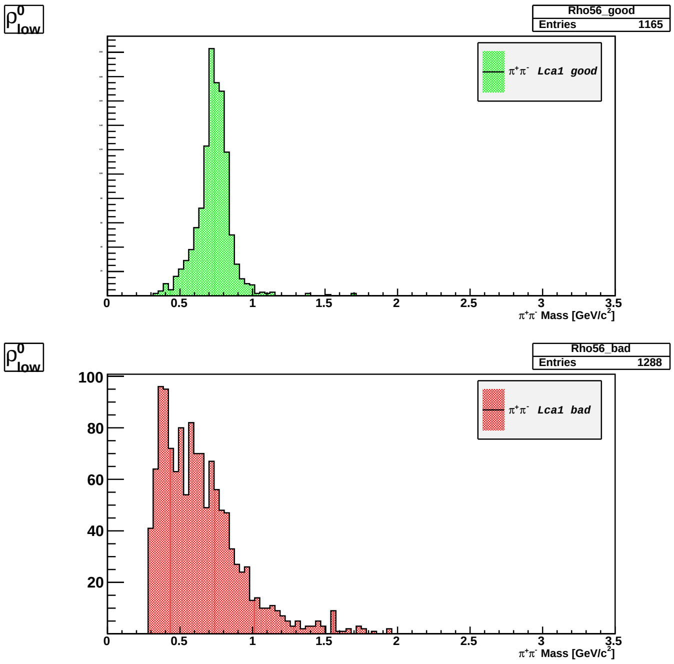

Figure D.9: *MC contributions to ρ^0_{low} from $\Lambda_b^0 \to \Lambda_c^+ a_1(1260)^-$ decay.*

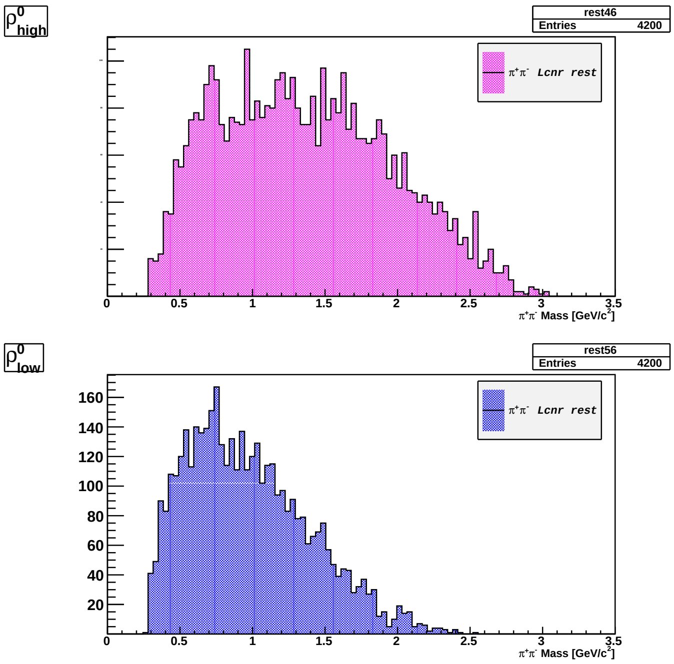

Figure D.10: *MC contributions to ρ^0_{high} (top) and to ρ^0_{low} (bottom) from $\Lambda_b^0 \to \Lambda_c^+\pi^-\pi^+\pi^-(nr)$ decay.*

D.3.2 Fit of Single Combinations

We made the fit on the weighted dataset of the ρ^0_{high} and ρ^0_{low} distributions of Fig. D.5(a) and Fig. D.5(b) modeling the contributions of the three decay modes with the corresponding PDFs of Fig. D.11, letting free to float in the fit their contribution. The fact that in principle there can be two different combinations of a pion pair, is a reason to make the fit of one of the two combinations (ρ^0_{high}, having the best mass resolution) and to use the achieved results, in terms of composition, as a cross-check on the other one, in order to verify that the fit of the $\pi^-\pi^+$ mass projection on the weighted dataset for ρ^0_{low} and ρ^0_{high} leads to the same results within the uncertainty.
The best fit result is reported respectively in Fig. D.12(a) for the ρ^0_{high} and in Fig. D.12(b) for the ρ^0_{low} combinations.
These fits show a clear and obvious difficulty in separating the ρ^0 contribution from the $\Lambda_b^0 \to \Lambda_c^+ a_1(1260)^-$ candidates, where $a_1(1260)^- \to \rho^0\pi^-$ and $\rho^0 \to \pi^-\pi^+$, and the ones from the $\Lambda_b^0 \to \Lambda_c^+\rho^0\pi^-$ candidates, where $\rho^0 \to \pi^-\pi^+$.
For the best fit of the ρ^0_{high} ditribution, the total yield of $\Lambda_b^0 \to \Lambda_c^+ a_1(1260)^-$ and $\Lambda_b^0 \to \Lambda_c^+\rho^0\pi^-$ and the yield of the $\Lambda_b^0 \to \Lambda_c^+\pi^-\pi^+\pi^-$ (see the fit results legenda) agrees with the same yields as determined in Sec. D.3. The same is not true for the ρ^0_{low} best fit where the yields are differents and only the $\Lambda_b^0 \to \Lambda_c^+\rho^0\pi^-$ is compatible with a null contribution.
We did several checks about the modeling of the templates without success.
The problem seems to be related to a wrong modeling of the ρ^0_{low} invariant mass distribution, the one with the lowest momentum.

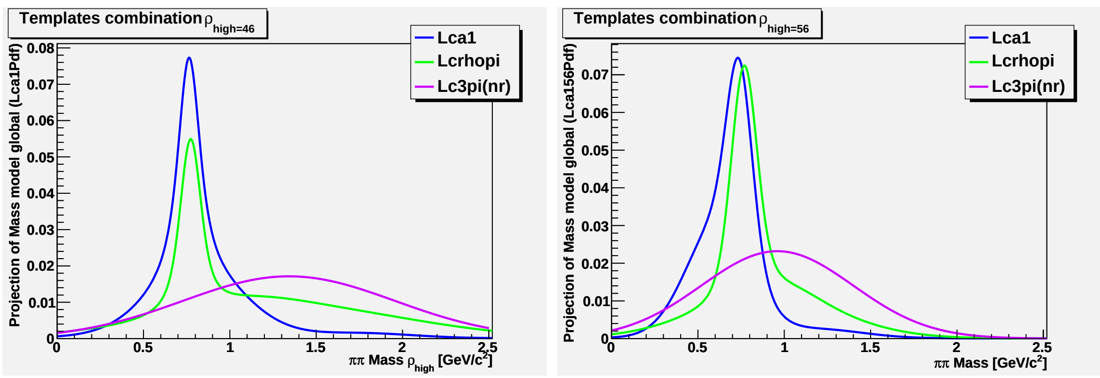

(a) (b)

Figure D.11: *MC templates used for the ρ^0_{high}* **D.11(a)** *and ρ^0_{low}* **D.11(b)** *contributions in the fit.*

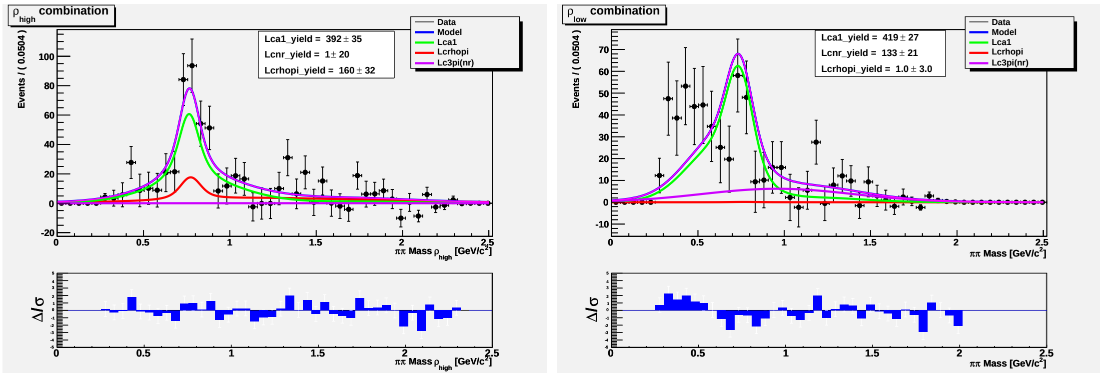

(a) (b)

Figure D.12: *Invariant mass distribution of ρ^0_{high}* **D.12(a)** *and ρ^0_{low}* **D.12(b)** *with overlaid the best fit curve (magenta curve).*

D.3.3 Final Considerations

The *s𝒫lot* technique, since it is an unbinned method, definitely gave us the possibility to derive the maximum information, because of the low statistics we have. Unfortunately the idea that make the fit of one of the two combinations (ρ^0_{high}, having the best mass resolution) and to use the achieved results in terms of composition as a cross-check on the other one, did not work.

Comparing the two fits separately (see Fig. D.12(a) and Fig. D.12(b)), we realize that the combination ρ^0_{high}, characterized by the π^- with highest momentum, is one that gives less problems in the fit. Furthermore, for the best fit of the ρ^0_{high} ditribution, the total yield of $\Lambda_b^0 \to \Lambda_c^+ a_1(1260)^-$ and $\Lambda_b^0 \to \Lambda_c^+\rho^0\pi^-$ and the yield of the $\Lambda_b^0 \to \Lambda_c^+\pi^-\pi^+\pi^-(nr)$ (see the fit results legenda) agrees with the same yields as determined in Sec. D.3 where a different method is used to extract the contributions of the sum of the $\Lambda_b^0 \to \Lambda_c^+ a_1(1260)^-$ and $\Lambda_b^0 \to \Lambda_c^+\rho^0\pi^-$, and of the $\Lambda_b^0 \to \Lambda_c^+\pi^-\pi^+\pi^-(nr)$. Since, Fig. D.5(c) clearly shows a peak due to the $a_1(1260)^-$, this decay definitively contributes to the $\Lambda_b^0 \to \Lambda_c^+\pi^-\pi^+\pi^-$ signal.

Despite all the studies done, we cannot exclude the $\Lambda_b^0 \to \Lambda_c^+\pi^-\pi^+\pi^-(nr)$ and we decided to continue this analysis (the update) assuming equal proportion (1/3, 1/3, 1/3) of the three decay modes.

Acronyms

SM Standard Model

LHC Large Hadron Collider

LHCb Large Hadron Collider beauty

CDF Collider Detector at Fermilab

CDF II CDF in Run II

FNAL Fermi National Accelerator Laboratory

V_{CKM} Cabibbo-Kobayashi-Maskawa matrix

CKM Cabibbo-Kobayashi-Maskawa

QCD Quantum Chromo Dynamics

RF Radio-frequency cavities

PDG Particle Data Group

SLAC Stanford Linear Accelerator Center

SVXII Silicon VerteX

ISL Intermediate Silicon Layers

L00 Layer ØØ

COT Central Outer Tracker

TOF Time Of Flight detector

CEM Central Electro Magnetic calorimeter

CES Central Electromagnetic Strip multi-wire proportional chambers

CPR Central Pre-Radiator

CHA Central HAdronic calorimeter

WHA Wall HAdronic calorimeter

PEM Plug ElectroMagnetic calorimeter

PHA Plug HAdronic calorimeter

CMU Central MUon detector

CMP Central Muon uPgrade

CMX Central Muon eXtension

IMU Intermediate MUon system

BMU Barrel MUon chambers

BSU Barrel Scintillation counters

TSU Toroid Scintillation counters

CLC Cherenkov Luminosity Counters

BC bunch-crossing

HQET Heavy Quark Effective Theory

XFT eXtremely Fast Tracker

SVT Silicon Vertex Trigger

DAQ Data AcQuisition System

MC Monte Carlo

TTT Two Track Trigger

CSL Consumer Server/Data Logger

VME Vesa Module Eurocard

PMT PhotoMultiplier Tube

OPE Operator Product Expansion

LEP Large Electron Positron

CP CP transformation that combines charge conjugation C with parity P

CERN Conseil Europen pour la Recherche Nuclaire

ALEPH Apparatus for LEP Physics (LEP Experiment)

DELPHI Detector with Lepton, Photon and Hadron Identification (LEP Experiment)

FMPS Fermilab Multiparticle Spectrometer

WE Weak Exchange diagram

CPU Central Processing Unit

PDF Probability Density Function

SPS Super Proton Synchrotron (CERN)

HERA Hadron Electron Ring Accelerator (DESY)

NLO Next-to-Leading Order

SVX Silicon VerteX

VLSI Very Large-Scale Integration

AM Associative Memory

TDC Time to Digital Converter

PID Particle Identification

CWA Central Wall HAdronic calorimeters

BR Branching Ratio

CS Cabibbo suppressed

CF Cabibbo favored

CL Confidence Level

rms Root Mean Square

XTRP eXTRaPolator unit

WLS wavelength shifters

HEPG High Energy Physics Group

Bibliography

[1] **K. Nakamura** and ***others*** **(Particle Data Group)**, "Review of Particle Physics," *J. Phys.* **G 37** *(2010) 075021*.

[2] **A. V. Manohar** and **M. B. Wise**, "Heavy quark physics," *Camb. Monogr. Part. Phys. Nucl. Phys. Cosmol.* **10** *(2000) 1*.

[3] **N. Isgur**, **D. Scora**, **B. Grinstein**, and **M. B. Wise**, "Semileptonic B and D Decays in the Quark Model," *Phys. Rev.* **D 39** *(1989) 799*.

[4] **I. Dunietz**, "CP violation with beautiful baryons," *Z. Physik* **C 56** *(1992) 129*.

[5] **A. K. Leibovich**, **Z. Ligeti**, **I. W. Stewart**, and **M. B. Wise**, "Predictions for nonleptonic Λ_b and Θ_b decays," *Phys. Lett.* **B 586** *(2004) 337*.

[6] **H.-Y. Cheng**, "Nonleptonic weak decays of bottom baryons," *Phys. Rev.* **D 56** *(1997) 2799*.

[7] **T. Aaltonen** and ***others*** **(CDF Collaboration)**, "First Measurement of the Ratio of Branching Fractions $\mathcal{B}(\Lambda_b^0 \to \Lambda_c^+ \mu^- \overline{\nu}_\mu$ / $\mathcal{B}(\Lambda_b^0 \to \Lambda_c^+ \pi^-)$," *Phys. Rev.* **D 79** *(2009) 032001*.

[8] **D. E. Acosta** and ***others*** **(CDF Collaboration)**, "Measurement of b hadron masses in exclusive J/ψ decays with the CDF detector," *Phys. Rev. Lett.* **96** *(2006) 202001*.

[9] **A. Abulencia** and ***others*** **(CDF Collaboration)**, "Measurement of the Λ_b^0 Lifetime in $\Lambda_b^0 \to J/\psi\Lambda^0$ in $p\bar{p}$ Collisions at $\sqrt{s} = 1.96\ TeV$," *Phys. Rev. Lett.* **98** *(2007) 122001*.

[10] **A. Abulencia** and ***others*** **(CDF Collaboration)**, "Measurement of $\sigma(\Lambda_b^0)/\sigma(\bar{B}^0) \times \mathcal{B}(\Lambda_b^0 \to \Lambda_c^+\pi^-)/\mathcal{B}(\overline{B^0} \to D^+\pi^-)$ in $p\bar{p}$ collisions at $\sqrt{s} = 1.96\,TeV$," *Phys. Rev. Lett.* **98** *(2007) 122002*.

[11] **T. Aaltonen** and ***others*** **(CDF Collaboration)**, "Measurement of Ratios of Fragmentation Fractions for Bottom Hadrons in $p\bar{p}$ Collisions at $\sqrt{s} = 1.96\,TeV$," *Phys. Rev.* **D 77** *(2008) 072003*.

[12] **T. Aaltonen**, **A. Abulencia**, and ***others*** **(CDF Collaboration)**, "Search for chargino-neutralino production in $p\bar{p}$ collisions at $\sqrt{s} = 1.96\,TeV$," *Phys. Rev. Lett.* **99** *(2007) 191806*.

[13] **T. Aaltonen**, **A. Abulencia**, **J. Adelman**, and ***others*** **(CDF Collaboration)**, "Observation and mass measurement of the baryon Ξ_b^-," *Phys. Rev. Lett.* **99** *(2007) 052002*.

[14] **T. Aaltonen** and ***others*** **(CDF Collaboration)**, "Observation of New Charmless Decays of Bottom Hadrons," *Phys. Rev. Lett.* **103** *(2009) 031801*.

[15] **P. Azzurri**, **P. Barria**, **M. A. Ciocci**, **S. Donati**, **P. Maestro**, and **E. Vataga**, "Measurement of $\mathcal{B}(\Lambda_b^0 \to \Lambda_c^+\pi^-\pi^+\pi^-)/\mathcal{B}(\Lambda_b^0 \to \Lambda_c^+\pi^-)$," *CDF Note 10563*.

[16] **P. Barria**, **P. Azzurri**, **M. A. Ciocci**, **S. Donati**, **P. Maestro**, and **E. Vataga**, "Measurement of $\mathcal{B}(\Lambda_b^0 \to \Lambda_c^+\pi^-\pi^+\pi^-)/\mathcal{B}(\Lambda_b^0 \to \Lambda_c^+\pi^-)$," *CDF Note 10564*.

[17] **R. Aaij** et al., "Measurements of the Branching fractions for $B_s \to D_s\pi\pi\pi$ and $\Lambda_b^0 \to \Lambda_c^+\pi\pi\pi$," *Phys. Rev.* **D 84** *(2011) 092001*.

[18] *CDF Web Page Analysis Blessed.* http://www-cdf.fnal.gov/physics/new/bottom/091029.blessed-Lb2Lc3pi-structure/LbLc3pi.html

[19] **P. Azzurri**, **P. Barria**, **M. A. Ciocci**, **S. Donati**, and **E. Vataga**, "First observation and measurement of the resonant structure of the $\Lambda_b^0 \to \Lambda_c^+\pi^-\pi^+\pi^-$ decay mode," *[arXiv:0912.4380]*.

[20] **F. Mandl** and **G. Shaw**, *Quantum Field Theory.* John Wiley & Son.

[21] **E. M. Peskin** and **D. V. Schroeder**, "An Introduction to quantum field theory," Addison-Wesley (1995) 842 p.

[22] **D. H. Perkins**, "Introduction to High-Energy Physics," Addison-Wesley (1982) 437p.

[23] **M. Kobayashi**, **H. Kondo**, and **T. Maskawa**, "Symmetry breaking of chiral u(3) x u(3) and x $\rightarrow \eta\ \pi\ \pi$ decay amplitude," *Prog. Theor. Phys.* **49** *(1973) 634, [doi:10.1143/PTP.49.634]*.

[24] **N. Cabibbo**, "Unitary symmetry and leptonic decays," *Phys. Rev. Lett.* **10** *(1963) 531, [doi:10.1103/PhysRevLett.10.531]*.

[25] **A. Sherstnev**, "Prospects for b-quark production cross section measurements in p p collisions at the LHC," *Nucl. Phys.* **167** *(Proc. Suppl.) (2007) 21,[arXiv:hep-ph/0609143]*.

[26] **A. D. Martin**, **W. J. Stirling**, and **R. G. Roberts**, "New information on parton distributions," *Phys. Rev.* **D 47** *(1993) 867*.

[27] **T. Sjostrand**, "Status of Fragmentation Models," *Int. J. Mod. Phys.* **A 3** *(1988) 751*.

[28] **S. Yu**, **R. Tesarek**, **D. Litvintsev**, **J. Heinrich**, and **N. Lockyer**, "Correction of $\Lambda_b^0 \rightarrow B^0$ Production Cross-Section Ratio," *CDF Note 7558*.

[29] **S. Yu**, **D. Litvintsev**, **R. Tesarek**, **J. Heinrich**, and **N. Lockyer**, "Ratio of $\mathcal{B}(\Lambda_b^0 \rightarrow \Lambda_c^+ \mu\nu) \rightarrow \mathcal{B}(\Lambda_b^0 \rightarrow \Lambda_c^+ \pi)$ in the two track trigger," *CDF Note 7559*.

[30] **S. Yu**, "First measurement of the ratio of branching fractions $\mathcal{B}(\Lambda_b^0 \rightarrow \Lambda_c^+ \mu\nu) \rightarrow \mathcal{B}(\Lambda_b^0 \rightarrow \Lambda_c^+ \pi^-)$," *CDF Thesis 7604*.

[31] **A. A. Affolder** and ***others*** **(CDF Collaboration)**, "Measurement of b quark fragmentation fractions in $p\bar{p}$ collisions at $\sqrt{s} = 1.8\ TeV$," *Phys. Rev. Lett.* **84** *(2000) 1663*.

[32] **C. Albajar** and ***others*** **(UA1 Collaboration)**, "First observation of the beauty baryon Λ_b^0 in the decay channel $\Lambda_b^0 \rightarrow J/\psi\Lambda$ at the CERN proton - anti-proton collider," *Phys. Lett.* **B 273** *(1991) 540*.

[33] **F. Abe** and ***others*** **(CDF Collaboration)**, "Search for $\Lambda_b \rightarrow J/\psi\Lambda^0$ in $p\bar{p}$ collisions at $\sqrt{s} = 1.8\ TeV$," *Phys. Rev.* **D 47** *(1993) 2639*.

[34] **P. Abreu** and ***others*** **(DELPHI Collaboration)**, "Search for exclusive decays of the Λ_b baryon and measurement of its mass," *Phys. Lett.* **B 374** *(1996) 351*.

[35] **F. Abe** and ***others*** **(CDF Collaboration)**, "Observation of $\Lambda_b^0 \rightarrow J/\psi\Lambda$ at the Fermilab proton antiproton collider," *Phys. Rev.* **D 55** *(1997) 1142*.

[36] **M. W. Arenton** and ***others*** , "Observation of massive $\Lambda K^0(s)\pi^+\pi^+\pi^-\pi^-$ events above 5 GeV/c^2," *Nucl. Phys.* **B 274** *(1986) 707*.

[37] **R. Barate** and ***others*** **(ALEPH Collaboration)**, "Measurement of the B baryon lifetime and branching fractions in Z decays," *Eur. Phys. J.* **C 2** *(1998) 197*.

[38] **J. Abdallah** and ***others*** **(DELPHI Collaboration)**, "Measurement of the Λ_b^0 decay form factor," *Phys. Lett.* **B 585** *(2004) 63*.

[39] **D. E. Acosta** and ***others*** **(CDF Collaboration)**, "Search for $\Lambda_b \to p\pi$ and $\Lambda_b \to pK$ decays in $p\bar{p}$ collisions at $\sqrt{s} = 1.96\,TeV$," *Phys. Rev.* **D 72** *(2005) 051104*.

[40] **D. E. Acosta** and ***others*** **(CDF Collaboration)**, "Search for radiative b-hadron decays in $p\bar{p}$ collisions at $\sqrt{s} = 1.8\;TeV$," *Phys. Rev.* **D 66** *(2002) 112002*.

[41] **K. G. Wilson**, "Nonlagrangian models of current algebra," *Phys. Rev.* **179** *(1969) 1499, [doi:10.1103/PhysRev.179.1499]*.

[42] **T. Appelquist** and **H. D. Politzer**, "Heavy quarks and e^+e^- annihilation," *Phys. Rev. Lett.* **34** *(1975) 43*.

[43] **E. Eichten** and **B. Hill**, "An effective field theory for the calculation of matrix elements involving heavy quarks," *Phys. Lett.* **B 234** *(1990) 511*.

[44] **U. Aglietti**, "Prediction of beauty particle masses with the heavy quark effective theory," *Phys. Lett.* **B 281** *(1992) 341*.

[45] **S. Godfrey** and **N. Isgur**, "Mesons in a Relativized Quark Model with Chromodynamics," *Phys. Rev.* **D 32** *(1985) 189, [doi:10.1103/PhysRevD.32.189]*.

[46] **N. Isgur** and **M. B. Wise**, "Weak Transition Form-Factors between Heavy Mesons," *Phys. Lett.* **B 237** *(1990) 527, [doi:10.1016/0370-2693(90)91219-2]*.

[47] **H. Georgi**, **B. Grinstein**, and **M. B. Wise**, "Λ_b semileptonic decay form factors for $m_c \neq \infty$," *Phys. Lett.* **B 252** *(1990) 456, [doi:10.1016/0370-2693(90)90569-R]*.

[48] **G. Aubrecht** and ***others*** , *A Teachers Guide To The Nuclear Science Wall Chart.* Contemporary Physics Education Project.

[49] **M. Popovic**, **L. Allen**, and **C. W. Schmidt**, "Fermilab Linac Injector, revisited," prepared for 16th IEEE Particle Accelerator Conference (PAC 95) and International Conference on High-energy Accelerators (IUPAP), Dallas, Texas, 1-5 May 1995.

[50] **D. Mohl**, "Physics and technique of stochastic cooling," *Phys. Reports*," vol. 58, 1980.

[51] **S. Nagaitsev** and ***others***, "Experimental demonstration of relativistic electron cooling," *Phys. Rev. Lett.* **96** *(2006) 044801*.

[52] **F. B. Division**, *RUN II Handbook*. http://www-bd.fnal.gov/lug/runII_handbook/RunII_index.html

[53] **D. Tonelli**, "First observation of the $B_s^0 \to K^+K^-$ decay mode, and measurement of the B^0 and B_s^0 mesons decay-rates into two-body, charmless final states at cdf," *CDF Thesis 8667*.

[54] **Collaboration CDF**, "The CDF IIb detector: Technical Design Report."

[55] **Collaboration CDF**, "The CDF II Detector Technical Design Report," October, 1996, summary of the CDF RunII Detector Parameters.

[56] **Collaboration CDF**, "Proposal for Ehnancement of the CDF II Detector: an Inner Silicon Layer and a Time of Flight Detector," October 23, 1998.

[57] **D. Acosta** and ***others***, "The performance of the CDF luminosity monitor," *Nucl. Instrum. Meth.* **A494** *(2002) 57*.

[58] **F. Abe** and ***others*** **(CDF Collaboration)**, "The CDF detector: an overview," *Nucl. Instrum. Meth.* **A271** *(1988) 387*, FERMILAB-PUB-94/024-E (1994).

[59] **R. Blair** and ***others*** **(CDF Collaboration)**, "The CDF II detector: Technical Design Report," FERMILAB-PUB-96/390-E (1996).

[60] **T. K. Nelson**, "The CDF Layer ØØ detector," *Int. J. Mod. Phys.* **A 16S1C** *(2001) 1091*.

[61] **A. Sill**, "CDF Run II silicon tracking projects," *Nucl. Instrum. Meth.* **A447** *(2000) 1*.

[62] **A. A. Affolder** and ***others***, "Status report of the intermediate silicon layers detector at CDFII," *Nucl. Instrum. Meth.* **A485** *(2002) 6*.

[63] **K. T. Pitts**, "The CDF Central Outer Tracker," *Nucl. Phys.* **61B** *(Proc. Suppl.) (1998) 230*.

[64] **C. S. Hill**, "Operational experience and performance of the CDFII silicon detector," *Nucl. Instrum. Meth.* **A530** *(2004) 1*.

[65] *Public Web Page*. http://penn01.fnal.gov

[66] **S. D'Auria**, **D. Lucchesi**, **S. Da Ronco**, **R. Carosi**, **M. Ciocci**, **S. Donati**, **P. Catastini**, **M. Morello**, **G. Punzi**, **P. Squillacioti**, **D. Tonelli**, **S. Torre**, **M. Rescigno**, **S. De Cecco**, **S. Giagu**, **M. Casarsa**, and **A. Cerri**, "Track-based calibration of the COT specific ionization," *CDF Note 6932*.

[67] **S. E. Yu**, "COT dE/dx measurement and corrections," *CDF Note 6361*.

[68] **P. Azzi**, **G. Busetto**, **P. Gatti**, and **A. Ribon**, "Histogram tracking in the COT," *CDF Note 5562*.

[69] **F. D. Snider**, "Tracking at CDF: Algorithms and experience from Run I and Run II," *Nucl. Instrum. Meth.* **A566** *(2006) 133*.

[70] **C. P. Hays** and ***others*** , "Inside-out tracking at CDF," *Nucl. Instrum. Meth.* **A538** *(2005) 249*.

[71] **J. Goldstein**, **C. Issever**, **T. Nelson**, **R. Snider**, and **D. Stuart**, "Silicon tracking for plug electrons," *CDF Note 5970*.

[72] **D. Acosta** and ***others*** **(CDF Collaboration)**, "A Time-Of-Flight detector in CDF-II," *Nucl. Instrum. Meth.* **A518** *(2004) 605*.

[73] **C. M. Ginsburg**, "CDF Run II Muon System," *Eur. Phys. J.* **C 33** *(2004) s1002*.

[74] **G. Ascoli** and ***others*** , "CDF central muon detector," *Nucl. Instrum. Meth.* **A268** *(1988) 33*.

[75] **S. Klimenko**, **J. Konigsberg**, and **T. M. Liss**, "Averaging of the inelastic cross sections measured by the CDF and the E811 experiments." http://lss.fnal.gov/archive/test-fn/0000/fermilab-fn-0741.pdf

[76] **G. Gomez-Ceballos** and ***others*** , "Event builder and Level 3 at the CDF experiment," *Nucl. Instrum. Meth.* **A518** *(2004) 522*.

[77] **T. Trigger** and **D. W. Group**, "Run II trigger table and datasets plan," *CDF Note 4718*.

[78] **E. J. Thomson** and ***others*** , "Online track processor for the CDF upgrade," *IEEE Trans. Nucl. Sci.* ***49**, 2002 (1063).*

[79] **A. Rahaman** and **R. Oldeman**, "Level-1 trigger rates of the two-track trigger at high-luminosities," *CDF Note 7370*.

[80] **S. R. Amendolia** and ***others*** , "The AMchip: a Full-custom CMOS VLSI Associative Memory for Pattern Recognition," *IEEE Trans. Nucl. Sci.* ***39**, 1992 (795).*

[81] **W. Ashmanskas** and ***others*** **(CDF Collaboration)**, "Performance of the CDF online silicon vertex tracker," *IEEE Trans. Nucl. Sci.* ***49**, 2002 (1177), [doi:10.1109/TNS.2002.1039633].*

[82] **R. Brun** and ***others*** , *GEANT: Simulation Program For Particle Physics Experiments. User Guide and Reference Manual.*

[83] **P. A. M. Fernandez**, "Performance of the CDF calorimeter simulation in Tevatron Run II," *AIP Conf. Proc.*," vol. 867, pp. 487–494, 2006.

[84] **R. Veenhof**, "Garfield, a drift chamber simulation program," prepared for International Conference on Programming and Mathematical Methods for Solving Physical Problems, Dubna, Russia, 14-19 Jun 1993.

[85] **R. Veenhof**, "GARFIELD, recent developments," *Nucl. Instrum. Meth.* **A419** *(1998) 726*.

[86] **W. Badgett**, "The CDF Run II Database and Online Java API," *CDF Note 5672*.

[87] **M. Ciocci**, **R. Tesarek**, and **E. Vataga**, "Datasets for fully reconstructed decays of $\Lambda_b^0 \to \Lambda_c^+\pi^-$ and $\Lambda_b^0 \to \Lambda_c^+\pi^-\pi^+\pi^-$," *CDF Note 9042*.

[88] **J. Marriner**, "Secondary vertex fit with mass and pointing constraints (CTVMFT)," *CDF Note 1996*.

[89] **K. Anikeev**, **P. Murat**, and **C. Paus**, "Description of Bgenerator II," *CDF Note 5092*.

[90] **D. Litvintsev** and ***others*** , "Measurement of the Λ_b^0 p_T spectrum in the Two Track Trigger data using fully reconstructed decay $\Lambda_b^0 \to \Lambda_c^+\pi^-$," *CDF Note 8156*.

[91] **W. Bell**, **J. P. Fernandez**, **L. Flores**, **F. Wuerthwein**, and **R. J. Tesarek**, *Users Guide to EvtGen at CDF.* http://www.slac.stanford.edu/lange/EvtGen

[92] **L. Aitala** and ***others*** , "Multidimendional Resonace Analysis of $\Lambda_c^+ \to pk^-\pi^+$," *Phys. Lett.* **B 471** *(2000) 449*.

[93] **W. Verkerke** and **D. Kirkby**, *RooFit Users Manual v2.07*. http://roofit.sourceforge.net/

[94] **A. E. Blechman**, **A. F. Falk**, **D. Pirjol**, and **J. M. Yelton**, "Threshold effects in excited charmed baryon decays," *Phys. Rev.* **D 67** *(2003) 074033*.

[95] **H. Albrecht** and ***others*** **(ARGUS Collaboration)**, "Search for Hadronic $b \to u$ decays," *Phys. Lett.* **B 241** *(1990) 278*.

[96] **B. Di Ruzza**, **L. Ortolan**, **G. Artoni**, **M. Dorigo**, **M. Rescigno**, and **A. Zanetti**, "Study of the $B_s^0 \to \phi\phi$ decay and measurement of its branching ratio," *CDF Note 9743*.

[97] **P. Azzurri**, **P. Barria**, **M. A. Ciocci**, **S. Donati**, **R. J. Tesarek**, and **E. Vataga**, "A Study of some Cabibbo suppressed Backgrounds to the Decay $\Lambda_b^0 \to \Lambda_c^+\pi^-\pi^+\pi^-$," *CDF Note 9845*.

[98] **W. Bell**, **J. P. Fernandez**, **L. Flores**, **F. Wuerthwein**, and **R. J. Tesarek**, "User Guide For EvtGen CDF," *CDF Note 5618*.

[99] **E. M. Aitala** and ***others*** **(E791 Collaboration)**, "Multidimensional resonance analysis of $\Lambda_c^+ \to pk^-\pi^+$," *Phys. Lett.* **B 471** *(2000) 449*.

[100] **M. Pivk** and **F. R. Le Diberder**, "$s\mathcal{P}lot$: a statistical tool to unfold data distributions," *Nucl. Instrum. Meth.* **A555** *(2005) 356*.

[101] **M. Šimečková**, "Maximum Weighted Likelihood Estimator in Logistic Regression," *WDS'05 Proceedings of Contributed Papers, Part I*, p. 144148, 2005.

List of Figures

1.1 Examples of $b\bar{b}$ production Feynman diagrams in a $p\bar{p}$ environments in a hadron collider. The reported processes are known as direct production, gluon fusion, flavor excitation and gluon splitting. . . . 6
1.2 Effect of a particle transverse momentum on the Λ_b^0 production fraction measurement: assuming the two distribution to be different, the fraction of measured Λ_b^0 depends on the p_T threshold. 7
1.3 Measurements of Λ_b^0 lifetime [1]: the lepton is an electron or a muon. 9
1.4 b-quark decay: **1.4(a)** b semileptonic decay and **1.4(b)** b hadronic decay. 10
1.5 Semileptonic $\Lambda_b^0 \to \Lambda_c^+ \ell \overline{\nu}_\ell$ and hadronic decay mode $\Lambda_b^0 \to \Lambda_c^+ \pi^-$: in the spectator model the b-quark decays weakly while the additional quark is a spectator to the Λ_b^0 baryon decay process. 11
1.6 Weak Exchange diagram for the $\Lambda_b^0 \to \Lambda_c^+ \pi^-$ decay mode. 12
1.7 Measurements of bottom hadron lifetimes [1]. 12

2.1 The figure compares the total cross section as function of the $\sqrt{s}$ for $pp \to X$ and $p\bar{p} \to X$ [1]. 17
2.2 The figure shows the accelerator system operating at FNAL. 18
2.3 Bunch structure of the Tevatron (BS = beam sync ticks = 132 ns). . 21
2.4 **2.4(a):** Integrated luminosity as a function of the time (or store number). The black curve is the luminosity delivered and the purple curve is luminosity written to tape. **2.4(b):** Initial luminosity as a function of the time (or store number). 23
2.5 The CDF II detector with a quadrant cut to expose the different subdetectors. 24
2.6 Elevation view of one half of the CDF II detector. 25
2.7 CDF coordinate system. 26
2.8 Schematic drawing of the impact parameter d_0. 27

2.9 Elevation view of one quadrant of the inner portion of the CDF II detector showing the tracking volume surrounded be the solenoid and the forward calorimeters. 28

2.10 The SVXII silicon detector. **2.10(a):** Three-dimensional view of the detector, showing the barrel structure along the beam axes. **2.10(b):** The transverse plane section shows in detail the layers sequence. 30

2.11 Silicon Detectors: $x - y$ and $z - y$ plane views. 31

2.12 A 1/6 section of the COT end-plate 2.12(a). For each super-layer is given the total number of cells, the wire orientation (axial or stereo), and the average radius in cm. The enlargement shows in details the slot where the wire planes (sense and field) are installed. Fig. 2.12 shows a sketch of an axial cross section of three cells in the superlayer 2, the arrow shows the radial direction. 32

2.13 Separation power of TOF for different particles at CDF, with dE/dx separation power for kaon and pion from COT superimposed. . . . 36

2.14 Elevation view of the CDF detector showing the components of the CDF calorimeter: CEM, CHA, WHA, PEM and PHA. 37

2.15 The plot show one azimuthal electromagnetic calorimeter wedge 2.15(a), the second plot shows an elevation view of one quarter of the plug calorimeter 2.15(b). 39

2.16 Muon detectors coverage in the $\eta - \varphi$ plane. 41

2.17 *Longitudinal section of the CLC system forward.* 43

2.18 *Block diagram showing the global trigger* **2.18(a)** *and the data flow for the L1 and L2 systems at CDF II* **2.18(b)**. 45

2.19 *Schematic chart showing the correlation between the tracks impact parameter (I.P.) and the decay length, in the transverse plane, of a hypothetical b-hadron decay.* 47

2.20 SVT architecture. 50

2.21 The plot shows the distribution of the impact parameter measured by SVT processor. 51

3.1 $\Lambda_b^0 \to \Lambda_c^+\pi^-$ **3.1(a)** and $\Lambda_b^0 \to \Lambda_c^+\pi^-\pi^+\pi^-$ **3.1(b)** event topology. 54

3.2 Block diagram of the skimming code (left) and a schematic of the Λ_b^0 recon- struction (right). 61

3.3 $\Lambda_c^+\pi^-\pi^+\pi^-$ **3.3(a)** and $\Lambda_c^+\pi^-$ **3.3(b)** candidates invariant mass after the skimming. $\Lambda_c^+\pi^-\pi^+\pi^-$ **3.3(c)** and $\Lambda_c^+\pi^-$ **3.3(d)** candidates invariant mass after the skimming and the optimized cuts. 64

3.4 Significance ($S/\sqrt{S+B}$) achieved in all the cut configurations scanned by the cut optimisation procedure. **Top left plot:** we have fixed $L_{xy}(\Lambda_b^0) > 200$ μm, the six big structures correspond to the six thresholds on the $L_{xy}(\Lambda_b^0)$ significance (10, 13, 15, 16, 18, 20); **Bottom left plot:** we have fixed $L_{xy}(\Lambda_b^0) > 200$ μm and $L_{xy}(\Lambda_b^0)/\sigma(L_{xy}(\Lambda_b^0)) >$ 16 the four big structures correspond to four cuts on $p_T(\Lambda_b^0)$ (7 GeV/c, 8 GeV/c, 9 GeV/c, 10 GeV/c); **Top right plot:** we have fixed $L_{xy}(\Lambda_b^0) > 200$ μm, $L_{xy}(\Lambda_b^0)/\sigma(L_{xy}(\Lambda_b^0)) > 16$ and $p_T(\Lambda_b^0) >$ 9 GeV/c, the four structures correspond to four cuts on $\mid d(\Lambda_b^0) \mid$ (60 μm, 70 μm, 80 μm, 90 μm); **Bottom right plot:** we have fixed $L_{xy}(\Lambda_b^0) > 200$ μm, $L_{xy}(\Lambda_b^0)/\sigma(L_{xy}(\Lambda_b^0)) > 16$, $p_T(\Lambda_b^0) > 9$ GeV/c and $\mid d(\Lambda_b^0) \mid < 70$ μm, the five points correspond to different cuts on $\Delta R(3\pi)$ (1.8, 1.6, 1.4, 1.2, 0.8). 65

3.5 ΔM^{--+} distribution after apply the offline selection and the optimized cuts. The distribution is modeled using as PDF the sum of an exponential (background) and a Gaussian (signal) functions.The best fit (blue curve) is overlaid to the experimental data (black points). 66

4.1 First order Feynman diagrams of the semileptonic decays $\Lambda_b^0 \rightarrow \Lambda_c^+(2595)^+\ell\overline{\nu}_\ell$ and $\Lambda_b^0 \rightarrow \Lambda_c^+(2625)^+\ell\overline{\nu}_\ell$. For these semileptonic decays, at the first order, only the spectator model diagram is allowed. 68

4.2 First order Feynman diagrams contributing to the hadronic decays $\Lambda_b^0 \rightarrow \Lambda_c(2595)^+\pi^-$ and $\Lambda_b^0 \rightarrow \Lambda_c(2625)^+\pi^-$. In the **4.2(a)** we have a Weak Exchange Feynman diagrams while in the **4.2(b)** the Spectator Model. 68

4.3 MC ΔM^{+-} distribution of all the $\Lambda_b^0 \rightarrow \Lambda_c^+\pi^-\pi^+\pi^-$ decay modes. The main contribution is due to $\Lambda_b^0 \rightarrow \Lambda_c(2595)^+\pi^-$ and $\Lambda_b^0 \rightarrow \Lambda_c(2625)^+\pi^-$ decay modes **4.3(a)** with respect to the others and in **4.3(b)** the logarithmic scale shows the limited contribution due to the others decay modes. 73

4.4 MC ΔM^{+} distribution of all the $\Lambda_b^0 \rightarrow \Lambda_c^+\pi^-\pi^+\pi^-$ decay modes after we vetoed $\Lambda_b^0 \rightarrow \Lambda_c(2595)^+\pi^-$ and $\Lambda_b^0 \rightarrow \Lambda_c(2625)^+\pi^-$ with the cut $\Delta M^{+-} > 0.380\,\mathrm{GeV/c^2}$. The main contribution is due to the $\Lambda_b^0 \rightarrow \Sigma_c(2455)^{++}\pi^-\pi^-$ signal in the region $\Delta M^{+} < 0.190\,\mathrm{GeV/c^2}$ **4.4(a)**. The logarithmic scale shows the limited contribution due to the others decay modes **4.4(b)**. 75

4.5 MC ΔM^- distribution of all the $\Lambda_b^0 \to \Lambda_c^+\pi^-\pi^+\pi^-$ decay modes after we vetoed $\Lambda_b^0 \to \Lambda_c(2595)^+\pi^-$ and $\Lambda_b^0 \to \Lambda_c(2625)^+\pi^-$ with the cut $\Delta M^{+-} > 0.380\,\mathrm{GeV/c^2}$. **4.5(a):** The $\Lambda_b^0 \to \Sigma_c(2455)^0\pi^+\pi^-$ is the main contribution the region $\Delta M^- < 0.190\,\mathrm{GeV/c^2}$, where the contribution of the other decay modes is negligible. **4.5(b):** The logarithmic scale enhances the limited contribution due to the other decay modes. 76

5.1 ΔM^{--+} mass distribution. **5.1(a):** The distribution is modeled using as PDF the sum of an exponential (background) and a Gaussian (signal) functions. Best fit (blue curve) is overlaid. **5.1(b):** Best fit (black curve), in the high mass region $[3.6 - 4.01]$ GeV/c^2, where only the combinatorial background contributes: the modeling in the fit uses an exponential as PDF. 80

5.2 ΔM^{--+} distribution with overlaid the best fit (blue curve). In the modeling the exponential shape is fixed to the shape determined from the fit in the high mass region: **5.2(a):** $\overline{B}^0 \to D^{(*)+}\pi^-\pi^+\pi^-$ and $\overline{B}^0_{(s)} \to D^{(*)+}_{(s)}\pi^-\pi^+\pi^-$ contributions (green line) are used to model the physical background. The $D^{(*)+}$ and $D^{(*)+}_{(s)}$ decay modes are inclusive. **5.2(b):** $\overline{B}^0 \to D^{(*)+}\pi^-\pi^+\pi^-$, $\overline{B}^0_{(s)} \to D^{(*)+}_{(s)}\pi^-\pi^+\pi^-$, and the $B^0 \to$ Inclusive contributions (green line) are used to model the background. **5.2(c):** same as in Fig. 5.2(a) but in $[3.2 - 3.6\,]GeV/c^2$ ΔM^{--+} range. **5.2(d):** same as in Fig. 5.2(b) but in $[3.2 - 3.6\,]GeV/c^2$ ΔM^{--+} range. 82

5.3 ΔM^{+-} distribution for the candidates in the Λ_b^0 $\pm 3\sigma$ mass window region with overlaid the best fit (blue curve) **5.3(a)** and ΔM^{--+} distribution when $\Delta M^{+-} < 0.380$ GeV/c^2 **5.3(b)** with overlaid the best fit distribution (blue curve) and the background contribution (green curve). 84

5.4 **5.4(a):** ΔM^{--+} distribution made for candidates when $\Delta M^{+-} < 0.325\,\mathrm{GeV/c^2}$ in order to select the $\Lambda_b^0 \to \Lambda_c(2595)^+\pi^-$ decay mode, with overlaid the best fit distribution (blue curve) and the contributing background (green curve). **5.4(b):** ΔM^{--+} distribution made for candidates in the $0.325\,\mathrm{GeV/c^2} < \Delta M^{+-} < 0.380\,\mathrm{GeV/c^2}$ window in order to select the $\Lambda_b^0 \to \Lambda_c(2625)^+\pi^-$ decay mode, with overlaid the best fit distribution (blue curve) and the contributing background (green curve). 85

5.5 ΔM^{+} distribution of the $\Sigma_c(2455)^{++}$ candidates in the Λ_b^0 left sideband region with overlaid the best fit (blue curve). In the fit in **5.5(a)** both Breit-Wigner width and the Gaussian resolution are floating while in **5.5(b)** the Breit-Wigner width is fixed to the PDG value and the Gaussian resolution is floating and determined by the fit. 86

5.6 **5.6(a):** ΔM^{+} distribution of the $\Sigma_c(2455)^{++}$ with overlaid the best fit (blue curve) - **particles 5.6(a)** and $\Sigma_c(2455)^{--}$ - **antiparticles 5.6(b)** in the left sideband region. 87

5.7 **5.7(a):** ΔM^{+} distribution of the $\Sigma_c(2455)^{++}$ candidates in the $\Lambda_b^0 \pm 3\sigma$ mass window with the resonances $\Lambda_c(2595)^{+}$ and $\Lambda_c(2625)^{+}$ vetoed with the cut $\Delta M^{+-} > 0.380\,\mathrm{GeV/c^2}$. The Gaussian resolution has been fixed to $1.0\,\mathrm{MeV/c^2}$. **5.7(b):** ΔM^{--+} distribution in the $\Sigma_c(2455)^{++}$ signal mass window $160\,\mathrm{MeV/c^2} < \Delta M^{+} < 176\,\mathrm{MeV/c^2}$. 87

5.8 ΔM^{-} distribution of the $\Sigma_c(2455)^{0}$ candidates in the left Λ_b^0 sideband region: **5.8(a):** The Voigtian PDF has a Gaussian constraint on the Breit-Wigner width and a floating resolution. **5.8(b):** The Breit-Wigner width in Voigtian PDF is fixed to the PDG value. The Gaussian sigma (`Q_S` in the top left, fit results legenda) as returned by the fit agrees with the one determined in Fig. 5.8(a). 88

5.9 ΔM^{-} distribution of the $\Sigma_c(2455)^{0}$ candidates in the left sideband region for **particles 5.9(a)** and **antiparticles 5.9(b)** with overlaid the best fit (blue curve). **5.9(c):** ΔM^{-} distribution corresponding to $\Sigma_c(2455)^{0}$ resonance in the Λ_b^0 mass window with $\Lambda_c(2595)^{+}$ and $\Lambda_c(2625)^{+}$ vetoed, with overlaid the best fit (blue curve). **5.9(d):** ΔM^{--+} distribution in the $\Sigma_c(2455)^{0}$ signal mass window $160\,\mathrm{MeV/c^2} < \Delta M^{+} < 176\,\mathrm{MeV/c^2}$ with overlaid the best fit (blue curve). 90

5.10 ΔM^{--+} distribution in [3.05-4.01]GeV/c^2 **5.10(a)** and in [3.2-4.01]GeV/c^2 **5.10(b)** mass range, with charmed resonant decay modes removed with the cuts $\Delta M^{+-} > 0.380\,\mathrm{GeV/c^2}$, $\Delta M^{+} > 0.190\,\mathrm{GeV/c^2}$ and $\Delta M^{-} > 0.190\,\mathrm{GeV/c^2}$ with overlaid the best fit (blue curve). The background modeling assumes an exponential with floating contribution and fixed slope plus the floating contribution of the $\overline{B}^0_{(s)} \rightarrow D^{(*)+}_{(s)}\pi^-\pi^+\pi^-$ (with inclusive $D^{(*)+}_{(s)}$ decays) templates and the floating contribution of the template of the $B^0 \rightarrow$ Inclusive decay; the best fit contribution is overlaid (green curve). 91

6.1 A plot schematically representing the set of selection requirements of the trigger (phase space) versus the effective trigger prescale. . . 99

7.1 **7.1(a):** ΔM^{+-} distribution of the CF $\Lambda_b^0 \to \Lambda_c(2595)^+\pi^-$ and CS $\Lambda_b^0 \to \Lambda_c(2595)^+K^-$; **7.1(b):** ΔM^{+-} distribution of the CF $\Lambda_b^0 \to \Lambda_c(2625)^+\pi^-$ and CS $\Lambda_b^0 \to \Lambda_c(2625)^+K^-$; **7.1(c):** ΔM^{+} distribution of the CF $\Lambda_b^0 \to \Sigma_c(2455)^{++}\pi^-\pi^-$ and CS $\Lambda_b^0 \to \Sigma_c(2455)^{++}\pi^-K^-$; **7.1(d):** ΔM^{-} distribution of the CF $\Lambda_b^0 \to \Sigma_c(2455)^0\pi^+K^-$ and CS $\Lambda_b^0 \to \Sigma_c(2455)^0\pi^+K^-$; . . . 112

7.2 **7.2(a):** ΔM^{--+} distribution of the CF $\Lambda_b^0 \to \Lambda_c(2595)^+\pi^-$ and CS $\Lambda_b^0 \to \Lambda_c(2595)^+K^-$; **7.2(b):** ΔM^{--+} distribution of the CF $\Lambda_b^0 \to \Lambda_c(2625)^+\pi^-$ and CS $\Lambda_b^0 \to \Lambda_c(2625)^+K^-$; **7.2(c):** ΔM^{--+} distribution of the CF $\Lambda_b^0 \to \Sigma_c(2455)^{++}\pi^-\pi^-$ and CS $\Lambda_b^0 \to \Sigma_c(2455)^{++}\pi^-K^-$; **7.2(d):** ΔM^{--+} distribution of the CF $\Lambda_b^0 \to \Sigma_c(2455)^0\pi^+K^-$ and CS $\Lambda_b^0 \to \Sigma_c(2455)^0\pi^+K^-$; . . . 113

A.1 $\Lambda_b^0 \to \Lambda_c^+\pi^-$ reconstructed candidates in the data, and used for MC validation, with overlaid the best fit curve. . . . 134

A.2 $p_T(\Lambda_b^0)$ **A.2(a)** and $y(\Lambda_b^0)$ **A.2(b)** distributions for data (black) and MC (red). Bottom plots are the ratio data/MC. . . . 134

A.3 $L_{xy}(\Lambda_b^0)$ **A.3(a)** and $L_{xy}(\Lambda_b^0)/\sigma L_{xy}(\Lambda_b^0)$ **A.3(b)** distributions for data (black) and MC (red). . . . 135

A.4 $d_0(\Lambda_b^0)$ **A.4(a)** and $m(\Lambda_b^0)$ **A.4(b)** distributions for data (black) and MC (red). . . . 135

A.5 $\chi^2(\Lambda_b^0)$ **A.5(a)** and Prob$(\chi^2(\Lambda_b^0))$ **A.5(b)** distributions of the reconstructed Λ_b^0 decay vertex for data (black) and MC (red). . . . 136

A.6 $L_{xy}(\Lambda_c^+)$ **A.6(a)** and $p_T(\Lambda_c^+)$ **A.6(b)** distributions for data (black) and MC (red). . . . 136

A.7 p_T distributions of the four tracks produced in the $\Lambda_b^0 \to \Lambda_c^+\pi^-$ decay for data (black) and MC (red). . . . 137

A.8 d_0 distributions of the four tracks produced in the $\Lambda_b^0 \to \Lambda_c^+\pi^-$ decay for data (black) and MC (red). . . . 138

A.9 φ_0 distributions of the four tracks produced in the $\Lambda_b^0 \to \Lambda_c^+\pi^-$ decay for data (black) and MC (red). . . . 139

A.10 z_0 distributions of the four tracks produced in the $\Lambda_b^0 \to \Lambda_c^+\pi^-$ decay for data (black) and MC (red). . . . 140

A.11 η distributions of the four tracks produced in the $\Lambda_b^0 \to \Lambda_c^+\pi^-$ decay for data (black) and MC (red). . . . 141

A.12 $p_T(\Lambda_b^0)$ comparison between data and MC for events collected by the `B_CHARM_LOWPT` trigger **A.12(a)** and `B_CHARM_HIGHPT` trigger **A.12(b)**. . . . 141

B.1 ΔM^{--+} MC distribution of $\overline{B}^0_{(s)} \rightarrow D^{(*)+}_{(s)}\pi^-\pi^+\pi^-$ (with inclusive $D^{(*)+}_{(s)}$ decay modes). 143

B.2 ΔM^{--+} MC distribution of $\overline{B}^0 \rightarrow D^+\pi^-\pi^+\pi^-$ **B.2(a)** and $\overline{B}^0_s \rightarrow D^+_s\pi^-\pi^+\pi^-$ **B.2(b)** with D^+ and the D^+_s decays in three charged tracks. 144

B.3 **B.3(a):** Fit of all the Λ^0_b candidates when the resonant decay modes have been removed with the cuts $\Delta M^{+-} > 0.380$ GeV/c^2, $\Delta M^+ > 0.190$ GeV/c^2 and $\Delta M^- > 0.190$ GeV/c^2, the background is modeled using an exponential shape with slope and normalization free to float in the fit. **B.3(b):** Unlike the previous plots here have been also included the floating contribution due to $\overline{B}^0 \rightarrow D^{(*)+}\pi^-\pi^+\pi^-$ and $\overline{B}^0_s \rightarrow D^{(*)+}_s\pi^-\pi^+\pi^-$ (with inclusive $D^{(*)+}$ and $D^{(*)+}_s$ decays) with a fixed shape (MC template). 145

B.4 ΔM^{--+} MC distributions of $B^0 \rightarrow$ Inclusive **B.4(a)**, $\Lambda^0_b \rightarrow \Lambda^+_c\pi^-\pi^+\pi^-\pi^0$ **B.4(b)** and $\Lambda^0_b \rightarrow \pi^-\pi^+\ell\overline{\nu}_\ell$ **B.4(c)**. 146

B.5 **B.5(a):** D^+ signal reconstructed in data by assigning the kaon and pion masses to the Λ^+_c decay products. **B.5(b):** $\overline{B}^0 \rightarrow D^+\pi^-\pi^+\pi^-$ signal reconstructed in data by using the D^+ signal (to reconstruct this signal we applied the cut $\mid m(D^+) - 1.868 \mid < 0.022$ GeV/c^2). **B.5(c):** MC mass distribution of the Λ^+_c (from Λ^0_b) reconstructed as D^+. 148

B.6 **B.6(a):** Reconstructed ΔM^{--+} distribution of the MC sample of $\overline{B}^0_{(s)} \rightarrow D^+_{(s)}\pi^-\pi^+\pi^-$ signals in the expected proportions. **B.6(b):** Fit of all the Λ^0_b candidates: resonant decay modes removed with the cuts $\Delta M^{+-} > 0.380$ GeV/c^2, $\Delta M^+ > 0.190$ GeV/c^2 and $\Delta M^- >$ 0.190 GeV/c^2 and the B^0 and B^0_s contribution fixed to 493 events. **B.6(c):** Fit of all the Λ^0_b candidates, including the the B^0 and B^0_s background left floating and determined by the fit. 149

C.1 Feynman diagram illustrating the decays $\Lambda^0_b \rightarrow \Sigma_c(2455)^0\pi^+\pi^-$ and $\Lambda^0_b \rightarrow \Sigma_c(2455)^0\pi^+K^-$. 153

C.2 Feynman diagrams illustrating the neutral *B-meson* decay modes corresponding to the baryonic decay mode on Fig. C.1. 153

C.3 Feynman diagrams illustrating the charged *B-meson* decay modes corresponding to the baryonic decay mode on Fig. C.1. 154

C.4 $\Lambda_c^+\pi^-\pi^+\pi^-$ invariant mass spectra for $\Lambda_b^0 \to \Lambda_c^+(2595)^+\pi^-$ and $\Lambda_b^0 \to \Lambda_c^+(2595)^+K^-$ **C.4(a)**, $\Lambda_b^0 \to \Lambda_c^+(2625)^+\pi^-$ and $\Lambda_b^0 \to \Lambda_c^+(2625)^+K^-$ **C.4(b)**, $\Lambda_b^0 \to \Sigma_c(2455)^{++}\pi^-\pi^-$ and $\Lambda_b^0 \to \Sigma_c(2455)^{++}\pi^-K^-$ **C.4(c)** and $\Lambda_b^0 \to \Sigma_c(2455)^0\pi^+\pi^-$ and $\Lambda_b^0 \to \Sigma_c(2455)^0\pi^+K^-$ **C.4(d)** resonant final states after the trigger and $\Lambda_c^+\pi^-\pi^+\pi^-$ selection. 161

C.5 $\Lambda_c^+\pi^-\pi^+\pi^-$ invariant mass spectra for $\Lambda_b^0 \to \Lambda_c^+\rho^0\pi^-$ and $\Lambda_b^0 \to \Lambda_c^+\rho^0K^-$ **C.5(a)** and $\Lambda_b^0 \to \Lambda_c^+\pi^-\pi^+\pi^-$ and $\Lambda_b^0 \to \Lambda_c^+\pi^-\pi^+K^-$ **C.5(b)** resonant final states after the trigger and $\Lambda_c^+\pi^-\pi^+\pi^-$ selection: the dashed line and the continuous one indicate the invariant mass distribution of the corresponding CF and CS decay modes reported in Tab. C.4. 162

C.6 $\Lambda_c^+\pi^-$ invariant mass for the decay mode $\Lambda_b^0 \to \Lambda_c^+\pi$ (Tab. C.4) after the trigger and $\Lambda_c^+\pi$ requirements. The dashed line and the continuous one indicate the invariant mass distribution of the corresponding CF and CS decay modes. 162

C.7 $\Lambda_c^+\pi^-\pi^+\pi^-$ invariant mass spectra for $\Lambda_b^0 \to \Lambda_c^+(2595)^+\pi^-$ and $\Lambda_b^0 \to \Lambda_c^+(2595)^+K^-$ **C.7(a)**, $\Lambda_b^0 \to \Lambda_c^+(2625)^+\pi^-$ and $\Lambda_b^0 \to \Lambda_c^+(2625)^+K^-$ **C.7(b)**, $\Lambda_b^0 \to \Sigma_c(2455)^{++}\pi^-\pi^-$ and $\Lambda_b^0 \to \Sigma_c(2455)^{++}\pi^-K^-$ **C.7(c)** and $\Lambda_b^0 \to \Sigma_c(2455)^0\pi^+\pi^-$ and $\Lambda_b^0 \to \Sigma_c(2455)^0\pi^+K^-$ **C.7(d)** resonant final states after trigger and Λ_c^+ 3π selection. 163

C.8 $\Lambda_c^+\pi^-\pi^+\pi^-$ invariant mass spectra for $\Lambda_b^0 \to \Lambda_c^+\rho^0\pi^-$ and $\Lambda_b^0 \to \Lambda_c^+\rho^0K^-$ **C.8(a)** and $\Lambda_b^0 \to \Lambda_c^+\pi^-\pi^+\pi^-$ and $\Lambda_b^0 \to \Lambda_c^+\pi^-\pi^+K^-$ **C.8(b)** resonant final states after trigger and Λ_c^+ 3π selection: the dashed line and the continuous one indicate the invariant mass distribution of the corresponding CF and CS decay modes that are reported in Tab. C.4. 164

C.9 $\Lambda_c^+\pi^-$ invariant mass for the decay $\Lambda_b^0 \to \Lambda_c^+\pi$ in Tab. C.4 after the trigger and $\Lambda_c^+\pi^-$ selection. The dashed line indicate the invariant mass distribution of the corresponding CF decay. 164

D.1 ΔM^{--+} distribution with indicated the mass window (MW) and the sideband (SB) used in the text. 166

D.2 $M_{\rho^0_{high}}$ **D.2(a)** and $M_{\rho^0_{low}}$ **D.2(b)** $\pi^+\pi^-$ invariant mass distribution in the mass window (red filled histogram) and in the sideband (yellow filled histogram) after vetoed the Λ_b^0 charmed resonant decay modes. 168

D.3 $M_{\rho^0_{high}}$ mass distribution with overlaid the best fit curve (magenta curve) in the mass window **D.3(a)** and in the sideband **D.3(b)** in range $[0.3 - 2.6]$ GeV$/c^2$. 168

D.4 $M_{\rho^0_{low}}$ mass distribution fit with overlaid the best fit curve (magenta curve) in the mass window **D.4(a)** and in the sideband **D.4(b)** in range $[0.3-2.6]$ GeV/c^2. 170
D.5 ρ^0_{high} **D.5(a)**, ρ^0_{low} **D.5(b)** and $m3\pi$ **D.5(c)** invariant mass projections on the weighted dataset. 172
D.6 MC contributions to ρ^0_{high} from $\Lambda^0_b \to \Lambda^+_c \rho^0 \pi^-$ decay. 174
D.7 MC contributions to ρ^0_{low} from $\Lambda^0_b \to \Lambda^+_c \rho^0 \pi^-$ decay. 175
D.8 MC contributions to ρ^0_{high} from $\Lambda^0_b \to \Lambda^+_c a_1(1260)^-$ decay. 175
D.9 MC contributions to ρ^0_{low} from $\Lambda^0_b \to \Lambda^+_c a_1(1260)^-$ decay. 176
D.10 MC contributions to ρ^0_{high} (top) and to ρ^0_{low} (bottom) from $\Lambda^0_b \to \Lambda^+_c \pi^- \pi^+ \pi^- (nr)$ decay. 176
D.11 MC templates used for the ρ^0_{high} **D.11(a)** and ρ^0_{low} **D.11(b)** contributions in the fit. 177
D.12 Invariant mass distribution of ρ^0_{high} **D.12(a)** and ρ^0_{low} **D.12(b)** with overlaid the best fit curve (magenta curve). 178

List of Tables

1 CDF b-Baryon measurements (Run II). xii

1.1 Observed lepton properties in the SM [1]. 2
1.2 Observed quark properties in the SM [1]. 3
1.3 This table compares the production rate of $b\bar{b}$ pairs in different environment. These numbers don't take into account experimental efficiencies for their detection. 5
1.4 UA1 measurement. 7
1.5 CDF measurements for the process $\Lambda_b^0 \to J/\psi\Lambda$. 8
1.6 Λ_b^0 information quoted from PDG [1]. The lepton is an electron or a muon. 8

2.1 Chronological overview of the Tevatron operation and performance. The fourth column reports the peak luminosity. The fifth column reports the delivered integrated luminosity. The last row shows the best performance as of this writing. 16
2.2 *Accelerator nominal parameters for Run II configuration.* 22
2.3 Relevant parameters for the layout of the sensors of the five SVXII layers. 30
2.4 Summary of the main characteristics of the CDF II calorimeter system. 39

3.1 `B_CHARM_LOWPT`, `B_CHARM_HIGHPT`, `B_CHARM_SCENA` trigger paths requirements. 57
3.2 Production output datasets used as input for skimming. 59
3.3 Output datasets from skimming and their relative sizes. 60
3.4 Tracks selection criteria. 60
3.5 $\Lambda_c^+ \to pK^-\pi^+$ and $\Lambda_b^0 \to \Lambda_c^+\pi^-\pi^+\pi^-$ candidates selection criteria. . 62
3.6 Optimised cuts used to select the $\Lambda_b^0 \to \Lambda_c^+\pi^-\pi^+\pi^-$ decay mode. . . 66

4.1 Decay modes of Λ_b^0 into $\Lambda_c^+\pi^-\pi^+\pi^-$ final state, with Λ_c^+ into $pK^-\pi^+$. 70

4.2 List of $\Lambda_c^+ \to pK^-\pi^+$ resonant and direct decay modes and measured BRs in percent [1]. The total branching ratio of $\Lambda_c^+ \to pK^-\pi^+$ is $(5.0 \pm 1.3)\%$. . . . 70
4.3 Decay modes of the $\Lambda_c(2595)^+$, $\Lambda_c(2625)^+$, $\Sigma_c(2455)^{++}$, $\Sigma_c(2455)^0$ and the BRs assumed in the simulation corresponding to their central value in the PDG [1]. . . . 71
4.4 Variables used to identify resonant charmed baryons in the decays of Λ_b^0 candidates and to separate them from the other Λ_b^0 decay modes. 72
4.5 Decay modes efficiency in percent after the cut $\Delta M^{+-} < 0.380\,\mathrm{GeV/c^2}$. 74
4.6 Efficiency on Λ_c^+ resonances after the veto on $\Delta M^{+-} > 0.380\,\mathrm{GeV/c^2}$. 74
4.7 Decay modes efficiency in percent after the veto on Λ_c^+ resonances and requiring $\Delta M^{+} < 0.190\,\mathrm{GeV/c^2}$. . . . 75
4.8 Decay modes efficiency in percent after the veto on Λ_c^+ resonances and requiring $\Delta M^{-} < 0.190\,\mathrm{GeV/c^2}$. . . . 76
4.9 Decay modes efficiency in percent after the veto on Λ_c^+ resonances and requiring $\Delta M^{+-} > 0.380\,\mathrm{GeV/c^2}$, $\Delta M^{+} > 0.190\,\mathrm{GeV/c^2}$, and $\Delta M^{-} > 0.190\,\mathrm{GeV/c^2}$. . . . 77
4.10 ΔM^{+-}, ΔM^{+} and ΔM^{-} cuts used to select the $\Lambda_b^0 \to \Lambda_c^+\pi^-\pi^+\pi^-$ decay modes. . . . 77

5.1 Experimental masses [1], mass differences with respect to Λ_c^+ mass and widths for the charmed resonances [1] described in the text. . . 83
5.2 Yields estimated by fitting the ΔM^{+-}, ΔM^{+} and ΔM^{-} distribution of the resonant candidates, in the Λ_b^0 mass region. The last row reports the yield of the $\Lambda_b^0 \to \Lambda_c^+\pi^-\pi^+\pi^-$ with the charmed resonances vetoed. The dataset is given by the two trigger paths `B_CHARM_LOWPT` and `B_CHARM`; the applied cuts are the optimised cuts with trigger confirmation. . . . 84

6.1 Absolute efficiencies for the three trigger scenarios (trigger confirmation+optimized cuts). We used "ScLow" for `B_CHARM_LOWPT`, "ScA" for `B_CHARM`, and "ScC" for `B_CHARM_HIGHPT`. . . . 97
6.2 Relative efficiencies for `B_CHARM_LOWPT` (*ScLow*), `B_CHARM` (*ScA*) and `B_CHARM_HIGHPT` (*ScC*) triggers scenarios, computed using simply the absolute efficiencies reported in Tab. 6.1. Quoted errors are statistical. Relative efficiencies average between `B_CHARM_LOWPT` and `B_CHARM` (*ScLow+ScC*) where the first uncertainty is statistical while the second one is the maximum difference between the average value and the single value and it is taken as the systematic uncertainty due to the average. . . . 98

6.3 Relative Branching Fractions in % measured in this work of Thesis. In these measurements the first uncertainty is statistical and the second one is systematic. 101
6.4 Relative branching fractions of the charmed resonant decay modes assuming no separation between $\Lambda_c^+\rho^0\pi^-$ and non resonant $\Lambda_c^+\pi^-\pi^+\pi^-(nr)$ or $\Lambda_c^+a_1(1260)^-$ decay modes. 102
6.5 Estimate of the relative branching fraction $\mathcal{B}(\Lambda_b^0 \to \Lambda_c^+\rho^0\pi^- + \Lambda_b^0 \to \Lambda_c^+\pi^-\pi^+\pi^-(other) \to \Lambda_c^+\pi^-\pi^+\pi^-)/\mathcal{B}(\Lambda_b^0 \to \Lambda_c^+\pi^-\pi^+\pi^-(all))$ assuming no separation between $\Lambda_c^+\rho^0\pi^-$ and non resonant $\Lambda_c^+\pi^-\pi^+\pi^-(nr)$ or $\Lambda_c^+a_1(1260)^-$ decay modes. 103
6.6 Measurement of the relative branching fraction $\mathcal{B}(\Lambda_b^0 \to \Lambda_c(2595)^+\pi^- \to \Lambda_c^+\pi^-\pi^+\pi^-)/\mathcal{B}(\Lambda_b^0 \to \Lambda_c(2625)^+\pi^- \to \Lambda_c^+\pi^-\pi^+\pi^-)$ assuming no separation between $\Lambda_c^+\rho^0\pi^-$ and non resonant $\Lambda_c^+\pi^-\pi^+\pi^-(nr)$ or $\Lambda_c^+a_1(1260)^-$ decay modes. 104
6.7 Measurement of the relative branching fraction $\mathcal{B}(\Lambda_b^0 \to \Sigma_c(2455)^{++}\pi^-\pi^- \to \Lambda_c^+\pi^-\pi^+\pi^-)/\mathcal{B}(\Lambda_b^0 \to \Sigma_c(2455)^0\pi^+\pi^- \to \Lambda_c^+\pi^-\pi^+\pi^-)$ assuming no separation between $\Lambda_c^+\rho^0\pi^-$ and non resonant $\Lambda_c^+\pi^-\pi^+\pi^-(nr)$ or $\Lambda_c^+a_1(1260)^-$ decay modes. 105
6.8 Measurement of the relative branching fraction $\mathcal{B}(\Lambda_b^0 \to \Lambda_c(2625)^+\pi^- \to \Lambda_c^+\pi^-\pi^+\pi^-)/\mathcal{B}(\Lambda_b^0 \to \Sigma_c(2455)^{++}\pi^-\pi^- \to \Lambda_c^+\pi^-\pi^+\pi^-)$ assuming no separation between $\Lambda_c^+\rho^0\pi^-$ and non resonant $\Lambda_c^+\pi^-\pi^+\pi^-(nr)$ or $\Lambda_c^+a_1(1260)^-$ decay modes. 106

7.1 $\Lambda_b^0 \to \Sigma_c(2455)^{++}\pi^-\pi^-$ and $\Lambda_b^0 \to \Sigma_c(2455)^0\pi^+\pi^-$ yields changing the Gaussian resolution, σ, used in the Voigtian fitting functions of Sec. 5.2.2 and Sec. 5.2.3. 108
7.2 Yields of the charmed resonant decay modes for the threshold mass central value and at $\pm 1\sigma$. 110
7.3 Yields of CS decay modes expected in the Λ_b^0 mass window. 111
7.4 Numbers of $\Lambda_c(2595)^+ \to \Lambda_c^+\pi^+\pi^-$ MC events passing all the optimised selection cuts, including trigger confirmation and absolute efficiencies (in units of $\times 10^{-4}$). 115
7.5 Relative efficiencies for B_CHARM_LOWPT, B_CHARM and for the average between B_CHARM_LOWPT and B_CHARM triggers scenarios, computed using the absolute efficiencies reported in Tab. 7.4. The quoted errors are the systematic uncertainties due to $\Lambda_c(2595)^+$ resonant structure. 115
7.6 Absolute efficiency of the $\Lambda_c(2625)^+ \to \Lambda_c^+\pi^+\pi^-$ decay mode when we assume $\mathcal{B}(\Lambda_c(2625)^+ \to \Sigma_c(2455)^{++}\pi^-) = 0.05$, $\mathcal{B}(\Lambda_c(2625)^+ \to \Sigma_c(2455)^0\pi^+) = 0.05$ and $\mathcal{B}(\Lambda_c(2625)^+ \to \Lambda_c^+\pi^+\pi^-) = 0.9$. 116

7.7 Relative efficiencies of the $\Lambda_c(2625)^+ \to \Lambda_c^+\pi^+\pi^-$ decay mode when we assume $\mathcal{B}(\Lambda_c(2625)^+ \to \Sigma_c(2455)^{++}\pi^-) = 0.05$ and $\mathcal{B}(\Lambda_c(2625)^+ \to \Sigma_c(2455)^0\pi^+) = 0.05$ and $\mathcal{B}(\Lambda_c(2625)^+ \to \Lambda_c^+\pi^+\pi^-) = 0.9$. 116

7.8 Absolute efficiencies of the $\Lambda_b^0 \to \Lambda_c^+\rho^0\pi^-$, $\Lambda_b^0 \to \Lambda_c^+\pi^-\pi^+\pi^-(nr)$, and $\Lambda_b^0 \to \Lambda_c^+ a_1(1260)^-$ decay modes. "ScLow" is for `B_CHARM_LOWPT`, "ScA" is `B_CHARM`, and "ScC" is `B_CHARM_HIGHPT`. We use the only the ScLoW and ScA trigger paths 117

7.9 Absolute efficiencies for the three trigger scenarios (trigger confirmation+optimised cuts). Λ_b^0 lifetime is PDG lifetime. "ScLow" is for `B_CHARM_LOWPT`, "ScA" is `B_CHARM`, and "ScC" is `B_CHARM_HIGHPT`. The MC sample, used to estimate the efficiencies, has been generated using $p_T(\Lambda_b^0)$, $\tau(\Lambda_b^0)$ and $\tau(\Lambda_c^+)$ for the top box, and $p_T(B^0)$, $\tau(\Lambda_b^0)$ and $\tau(\Lambda_c^+)$ for the bottom one. 118

7.10 Relative efficiencies for `B_CHARM_LOWPT`, `B_CHARM` and `B_CHARM_HIGHPT` triggers scenarios, computed using simply the absolute efficiencies reported in Tab. 7.9. The third box reports the average values between `B_CHARM_LOWPT` and `B_CHARM` ($p_T(\Lambda_b^0)$, Λ_b^0 and Λ_c^+ lifetime is PDG lifetime). 119

7.11 Relative efficiencies for `B_CHARM_LOWPT`, `B_CHARM` and `B_CHARM_HIGHPT` triggers scenarios, computed using simply the absolute efficiencies reported in Tab. 7.9. The third box is the average between `B_CHARM_LOWPT` and `B_CHARM` (Λ_b^0 lifetime is PDG lifetime, $p_T(\Lambda_b^0)$ is taken as $p_T(B^0)$, Λ_b^0 and Λ_c^+ lifetime is PDG lifetime). 120

7.12 Scaling factor of the absolute efficiencies for the different combination of the polarizations and trigger scenarios. 121

7.13 Relative efficiencies computed assuming the "+ +" polarization combination. 122

7.14 Relative efficiencies computed assuming the "- +" polarization combination. 123

7.15 Relative efficiencies computed assuming the "+ -" polarization combination. 124

7.16 Relative efficiencies computed assuming the "- -" polarization combination. 125

7.17 Relative Branching Fractions in % measured in this work of Thesis. In these measurements the first uncertainty is statistical and the second one is systematic. 127

7.18 Relative Branching Fractions in % measured after the update [15]. In these measurements the first uncertainty is statistical and the second one is systematic. Here other indicates the sum of the $\Lambda_b^0 \to \Lambda_c^+\pi^-\pi^+\pi^-(nr)$ and of the $\Lambda_b^0 \to \Lambda_c^+ a_1(1260)^- \to \Lambda_c^+\rho^0\pi^- \to \Lambda_c^+\pi^-\pi^+\pi^-$. 128
7.19 Absolute branching fractions are derived by normalizing to the known value $\mathcal{B}(\Lambda_b^0 \to \Lambda_c^+\pi^-) = (8.8 \pm 3.2) \times 10^{-3}$ [1]. The first quoted uncertainty is statistical, the second is systematic, and the third is due to the uncertainty on the $\Lambda_b^0 \to \Lambda_c^+\pi^-$ branching fractions. Here other indicates the sum of the $\Lambda_c^+\pi^-\pi^+\pi^-(nr)$ and of the $\Lambda_b^0 \to \Lambda_c^+ a_1(1260)^- \to \Lambda_c^+\rho^0\pi^- \to \Lambda_c^+\pi^-\pi^+\pi^-$ 129

C.1 CF and CS decay modes. 152
C.2 List of CF and CS *B-meson* decay modes, the corresponding BR from PDG [1], baryonic Λ_b^0 decay modes and sum of BRs for the CF and CS associated *B-meson* decay modes. 156
C.3 Common requirements for the selection $\Lambda_b^0 \to \Lambda_c^+\pi^-$, $\Lambda_b^0 \to \Lambda_c^+\pi^-\pi^+\pi^-$ and corresponding CS decay modes. 158
C.4 MC efficiency after trigger (TTT) and analysis cuts. 159
C.5 For each decay mode is reported the number of passing events for CF ($\#events\ CF = N^i_{CF}$) and for CS ($\#events\ CS$), the number of the expected CS events ($\#events\ CS\ exp. = N^i_{CS}$) and the ratio N^i_{CS}/N^i_{CF} (scaling factor). 159
C.6 This summary reports, for each Λ_b^0 decay modes, the relative $\mathcal{B}$, the analysis efficiency, the relative efficiencies, and the product of $\Pi\ R_i(\varepsilon_i/\varepsilon_0)$, which for the i^{th} decay mode is the evaluated N^i_{CS}/N^i_{CF} (scaling factor for the i^{th} decay mode). 160

D.1 Some useful quantities determined using the best fit parameters of the ΔM^{--+} distribution of Fig. 5.10(b). 167
D.2 Yields of ρ^0_{high} and ρ^0_{low} in the MW and in the SB regions obtained from the best fit of $M_{\rho^0_{high}}$ and $M_{\rho^0_{low}}$ distributions reported in Fig. D.3(a) and Fig. D.3(b). The yield of the ρ^0_{high} (ρ^0_{low}) in the $\Lambda_b^0 \to \Lambda_c^+\pi^-\pi^+\pi^-$ is given by the difference between the yields ρ^0_{high} (ρ^0_{low}) in the MW and in the SB. 169
D.3 In this table we report the yield of the $\Lambda_b^0 \to \Lambda_c^+\pi^-\pi^+\pi^-$ after the veto on the charmed resonances (N_{TOT}), the yield of the ρ^0 (N_{ρ^0}) that in principle are due the $\Lambda_b^0 \to \Lambda_c^+\rho^0\pi^- \to \pi^-\pi^+\pi^-$ and $\Lambda_b^0 \to \Lambda_c^+ a_1(1260)^- \to \Lambda_c^+\rho^0\pi^- \to \pi^-\pi^+\pi^-$ decays, and the yield of the $\Lambda_b^0 \to \Lambda_c^+\pi^-\pi^+\pi^-(nr)$ (N_{nr}). 170

Acknowledgements

Am I dreaming or is it really over?

If I get here I think it is also the time to write "the end" to this adventure and to say thank you to all those who have been involved with me in this adventure. As it is well known to all, synthesis is not my best quality, but this time I'd surprise everyone.

I would like to start thanking my supervisor Agnese especially for this final multilanguage brain storming and for giving me the opportunity to know the CDF experiment but above all the CDF people.

A thank goes to my colleagues of the "Fellowship of the Lambda B" Elena Vataga, Paolo Azzurri, Rick Tesarek and Simone Donati. I really appreciate it, especially in difficult times.

This adventure would not be the same if I had not met Ciccio, Gerardo, Mr. Drive Foxes, Saba, Janu, Maria, Simpatia, Mr. Montecherlo, The Parmesan guy, The hungry guy, Betta, Svampi, Ricciotto, Marcolino, Pretty woman, Farunfi, Boss, Little Joint, and many other people who shared with me good and bad times.

Ciccio thanks for giving me unconsciously a challenge more or less every day.
Thanks Oscar for having done what someone else would have done.
Saba how can I do without you at home?

A special thanks goes to Paola, omnipresent in my life in these last days, taking care of me.

Bombolona, Manu, Bea, Stefy I have a message for you: "I'm still alive!".

A special thought goes to my 5 sigmas of happiness, Viviana, for sharing with me this PhD with all the complications. I couldn't have asked for a better "partner" to share travels and a lot of fun. I didn't tell you but all the "omissis" in this Thesis are dedicated to you. You have been really important for me and without you it would not be the same thing.
It will not be easy to get rid of me but you must not take it as a threat.
See you to the next challenge ... blindfolded archery .

Thanks also to my friends in Rome, Pisa and Fermilab.
Sorry guys if you don't see here your name but, as you know, I'm extremely inclusive and you are so many.

This thesis is dedicated to my family and in particular to my father, that always supported me and believed in me no matter the crazy choices I took and above all, despite the fact that these choices have let me go away.

Each of you gave me a lot of fun and since fun is important I will come to check you one by one no matter where you are. Since I'm The Ultimate Ace now it's time to close and write the word *The End* to this story. It will be difficult to forget each of you.

That's all folks!